

Europa

The Production of Oxidants in Europa's Surface

R.E. JOHNSON,¹ T.I. QUICKENDEN,² P.D. COOPER,² A.J. MCKINLEY,²
and C.G. FREEMAN³

ABSTRACT

The oxidants produced by radiolysis and photolysis in the icy surface of Europa may be necessary to sustain carbon-based biochemistry in Europa's putative subsurface ocean. Because the subduction of oxidants to the ocean presents considerable thermodynamic challenges, we examine the formation of oxygen and related species in Europa's surface ice with the goal of characterizing the chemical state of the irradiated material. Relevant spectral observations of Europa and the laboratory data on the production of oxygen and related species are first summarized. Since the laboratory data are incomplete, we examine the rate equations for formation of oxygen and its chemical precursors by radiolysis and photolysis. Measurements and simple rate equations are suggested that can be used to characterize the production of oxidants in Europa's surface material and the chemical environment produced by radiolysis. Possible precursor molecules and the role of radical trapping are examined. The possibility of oxygen reactions on grain surfaces in Europa's regolith is discussed, and the earlier estimates of the supply of O₂ to the atmosphere are increased. **Key Words:** Europa—Oxygen—Ice—Chemical kinetics. *Astrobiology* 3, 823–850.

INTRODUCTION

THE PUTATIVE SUBSURFACE OCEAN on Europa is of interest to astrobiologists as an environment that might be able to sustain life processes. Given the presence of oxygen, carbon, sulfur, and, possibly, nitrogen, organisms dependent on conventional carbon-based biochemistry may be feasible. However, the presence of aerobic life processes may be contingent on the transport of oxidants or oxygenated species formed at the surface to an ocean that is covered by a substantial thickness of ice (Chyba, 2000; Kargel *et al.*, 2000;

Chyba and Hand, 2001; Cooper *et al.*, 2001). Although oxygen has been detected in Europa's very thin atmosphere and oxidants have been observed as trapped species in its icy surface, their transport to a subsurface ocean presents considerable thermodynamic and kinetic challenges.

It is generally agreed that the radiolysis of ice by energetic ions and electrons trapped in the Jovian magnetosphere produces the oxygen and peroxide seen in Europa's icy surface (e.g., Johnson *et al.*, 2003). This occurs because the bombarding particles chemically alter the ice and decompose it, producing molecular hydrogen and oxygen.

¹Engineering Physics, University of Virginia, Charlottesville, Virginia.

²School of Biomedical and Chemical Sciences, University of Western Australia, Crawley, Australia.

³Department of Chemistry, University of Canterbury, Christchurch, New Zealand.

The hydrogen readily escapes from the surface material and, in turn, from Europa's atmosphere because of the low gravitational field. The options for oxygen are the release into the tenuous atmosphere, where it is retained because of its high molecular mass, and retention in the ice lattice as homogeneously dissolved oxygen, as trapped bubbles of oxygen, or as an oxidized trace species. Because of the preferential loss of hydrogen, oxygen-rich species are formed preferentially in Europa's surface ice (Johnson and Quickenden, 1997; Madey *et al.*, 2002). Therefore, oxygen, peroxide, and oxidized sulfur and carbon have been detected as trapped species (e.g., Johnson *et al.*, 2003).

The production and trapping of such species in the surface layers are, of course, not sufficient for our purposes, as indicated schematically in Fig. 1. Radiolysis can occur to depths of the order of tens of centimeters because of the penetration of the energetic component of the incident radiation (Cooper *et al.*, 2001; Paranicas *et al.*, 2001). Mixing of these radiolytic products to greater depths occurs because of meteoroid bombardment (Cooper *et al.*, 2001). This bombardment also produces a porous regolith (Buratti, 1995) composed of sintered grains (Grundy *et al.*, 2001), which increases the effective radiation penetration depth. In addition, the atmospheric O₂ permeates pore space in the regolith. Therefore, oxygen gas in the porous regolith can be trapped by the collapse of pores on meteoroid impact or can react on grain

surfaces well below the typical radiation penetration depth. Finally, macroscopic mass transport of trapped species by crustal subduction (Prockter and Pappalardo, 2000) must occur. Because of the temperature gradient, relevant species must be stable in the ice at temperatures well above Europa's surface temperature (80–110K) and at higher pressures. The subduction process effectively is a macroscopic mass transport pump, which is needed to carry oxidants to Europa's ocean.

As a first step, we focus in this paper on the chemical processes leading to the formation of oxygen and related oxidants in Europa's regolith. The goal is to characterize the chemical state and stability of the irradiated surface material. We first summarize the spacecraft and telescopic observations of oxygen and related species at Europa. Next we summarize the laboratory data on the radiolysis and photolysis of ice. Because data are not available for all incident species and incident energies, we concentrate on the descriptions of the chemistry of formation of molecular oxygen. The focus on oxygen is not because this is the species delivered to a subsurface ocean, but because understanding the chemistry of its formation in ice is key to describing the chemical state and stability of Europa's irradiated surface material. We then use the data to correct previous estimates of the production rate of oxygen at Europa and suggest experiments in order to characterize the chemical state of the irradiated surface that leads to the production of O₂.

OBSERVATIONS

Molecular oxygen

Tenuous oxygen atmospheres have been reported at both Ganymede (Hall *et al.*, 1998) and Europa (Hall *et al.*, 1995) based on Hubble Space Telescope (HST) observations. The detection of molecular oxygen was indirect. That is, two lines (135.6 and 130.4 nm) due to excited O were observed in emission, and their ratio (~1.9) suggested that the excited atoms were produced by electron impact dissociation of molecular oxygen. In addition, two well-known transitions for interacting pairs of O₂ molecules, ${}^1\Delta_g + {}^1\Delta_g \leftarrow {}^3\Sigma_g^- + {}^3\Sigma_g^-$, were observed in the reflectance spectra of Ganymede (Calvin *et al.*, 1995; Spencer *et al.*, 1995) and Europa (Spencer and Klesman,

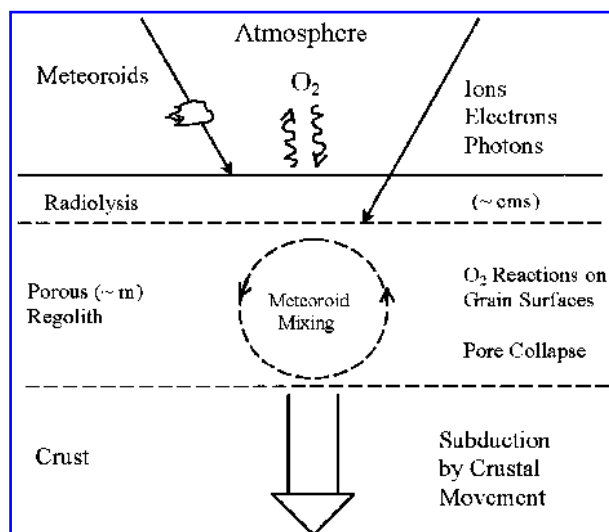


FIG. 1. Diagram of processes occurring on Europa's surface as discussed in the text.

2001; Spencer and Calvin, 2002) using ground-based telescopes and the HST. These absorption bands cannot be due to atmospheric O₂ because very high pressures or very long line-of-sight columns of O₂ would be required.

The positions of the two signature absorptions for dimer O₂, at 577.2 nm and 627.5 nm, respectively (Landau *et al.*, 1962; Cooper *et al.*, 2003a), suggest that the O₂ is locally quite dense (Calvin *et al.*, 1996, 2003). Therefore, these bands were suggested to be due to inclusions of O₂ trapped within Ganymede's icy surface (Calvin *et al.*, 1996; Johnson and Jessor, 1997). It is seen from Table 1 that although the atmospheric and surface reservoirs of O₂ are coupled, the oxygen content in the surface ice is the largest.

The observed O₂-dimer band shapes and relative band depths are distorted from solid or liquid O₂ (Johnson, 1999). At Ganymede, where spatial resolution was obtained using the HST, both the position of the band minimum and its shape vary with latitude (Calvin and Spencer, 1997). Therefore, care must be taken when comparing the peak positions of the bands seen in the discovery spectrum at Ganymede with those of solid or liquid oxygen. This spectrum is a hemispherical average of spectral features that vary in their peak positions and band shapes. It was obtained by ratioing Ganymede's reflectance to that of Callisto (Spencer *et al.*, 1995), which we now know exhibits a weak solid-like O₂ feature. It was recently shown that O₂ is also trapped in Europa's icy surface (Spencer and Klesman, 2001; Spencer and Calvin, 2002). However, the solid-like O₂ feature at Europa is much weaker than that at Ganymede (577.2 nm band depth ~0.3% vs. ~1.8%). This could be due to the fact that Europa's surface scatters light more efficiently in the visible, leading to shorter path lengths (Johnson and Jessor, 1997). It could also be due to compet-

ing chemical processes (Calvin *et al.*, 1996; Johnson and Quickenden, 1997).

Ozone and peroxide

Related to the oxygen observations, the Hartley band of O₃ has been tentatively identified in the ultraviolet (UV) reflectance spectra of Ganymede and in the icy satellites of Saturn (Noll *et al.*, 1996, 1997). O₃ trapped within the icy surface would be consistent with the presence of trapped oxygen exposed to radiolysis (Johnson and Quickenden, 1997). The presence of trapped O₃ supports the interpretation that the dimer-O₂ observations are due to inclusions of oxygen trapped in the ice. However, the shape of the O₃-like feature also varies significantly with latitude at Ganymede (Hendrix *et al.*, 1999a) and is highly distorted. Based on the band shape, the presence of an additional absorbing species was inferred. This was initially suggested to be trapped OH (~0.28 μm) (Noll *et al.*, 1996), but may more likely be due to organic molecules (Johnson, 2001). This O₃-like feature is superimposed on a very broad UV absorption extending from about 0.4 μm to shorter wavelengths seen on all of the icy satellites. The broad UV absorption has been attributed to another radiolytically produced oxidant, H₂O₂ (Carlson *et al.*, 1999a; Hendrix *et al.*, 1999b), but may also include absorption by trapped HO₂ and OH (Taub and Eiben, 1968; Johnson and Quickenden, 1997). Identification of specific radiolytic products in the UV is difficult because the bands are very broad and overlap. The presence of H₂O₂ trapped in Europa's ice was confirmed by a band in the infrared observed using the Near Infrared Mapping Spectrometer (NIMS) on the Galileo spacecraft (Carlson *et al.*, 1999a). Remarkably, the amount seen in the infrared is roughly consistent with the amount suggested by the decrease in reflected light in the UV.

TABLE 1. GLOBAL OXIDANT INVENTORY

Reservoir	Oxidant	Column density (10 ¹⁶ mol/cm ²)
Atmosphere ¹	O ₂	~0.10
Regolith (gas) ²	O ₂	~10 ⁻⁵
Trapped in ice (1 mm at unit density) ^{3,4}	O ₂	~50–500
	H ₂ O ₂	~400

¹Based on Hall *et al.* (1995, 1998).

²Estimated using average regolith depth of ~1 m.

³Europa band depth approximately one-sixth that in Calvin *et al.* (1996), who give 0.1–1% concentration on Ganymede.

⁴For comparison, sulfur species on the trailing hemisphere: [SO₂] ~300 [sulfate], or ~1,000 × 10¹⁶ mol/cm².

Whereas H_2O_2 is observed in ice at Europa at $\sim 0.13\%$ level, the O_3 -like UV feature seen at Ganymede is not obvious at Europa (e.g., Fanale *et al.*, 1999). This again may be due to the fact that less trapped O_2 is seen in reflectance at Europa than at Ganymede. That is, since O_2 is a precursor of O_3 , the factor of ~ 6 reduction in O_2 means that the identification of this broad feature superimposed on other broad UV bands is problematic. However, the absence of the O_3 -like feature could also be due to the presence of sulfur species that strongly compete for excess oxygen (Johnson and Quickenden, 1997).

Summary: space observations

Although each of the individual identifications of suggested products of water radiolysis or photolysis (OH , H_2O_2 , O_2 , O_3) has some uncertainty, the reflectance spectra taken as a whole give a fairly clear, self-consistent picture. The irradiated surfaces of the icy satellites contain trapped molecules that would be expected from radiolysis or photolysis of an icy surface (Johnson and Quickenden, 1997). Indeed, OH is a suggested precursor of H_2O_2 , which is a suggested precursor of O_2 , which in turn is a precursor of O_3 . However, the separation into amounts of individual species based on the absorption in the UV identifications remains difficult. Therefore, the observed band of trapped H_2O_2 in the infrared and the pair of bands in the visible of a condensed form of O_2 are critical, as they confirm the presence of radiolytically produced oxidizing molecules in Europa's icy surface.

Consistent with the above, oxygen-rich molecules derived from the radiation processing of an ice containing sulfur (SO_2 and a sulfate) and carbon (CO_2 and a carbonate) have been identified (see, e.g., Johnson *et al.*, 2003). The sulfate has been suggested to be a hydrated salt mineral (McCord *et al.*, 1999) or a hydrated sulfuric acid (Carlson *et al.*, 1999b, 2002). The latter is an efficient oxidant that is also refractory. Together these observations indicate that volatile and refractory oxidizing molecules are readily formed by radiolysis and photolysis in Europa's surface material. If indeed that material can be delivered to Europa's putative subsurface ocean, a source of free energy may be available for potential biological activity. Here we consider the formation of molecular oxidants by radiolysis with emphasis on O_2 .

RADIOLYTIC PRODUCTION: LABORATORY DATA

Introduction

In this section we review the laboratory data leading to the production of oxygen and related species by radiolysis and photolysis of ice. We first compare the data for production of oxygen by incident ions, electrons, and UV photons. This is followed by a review of the data on the loss of hydrogen, which is the other principal product of radiation-induced decomposition of ice. We then consider the evidence that certain proposed species, such as peroxide or trapped O, might be precursors to molecular oxygen formation in ice. Some of these data have been summarized earlier, but with a very different emphasis. Here the goal is to motivate the development of chemical models for describing irradiated ice, models that can be used to suggest new experiments and to interpret data. Individuals familiar with the data can go directly to the modeling section, in which rate equations are developed and used to interpret aspects of the diverse database.

Molecular oxygen

Gas-phase O_2 has been produced by irradiating low temperature ice using UV photons, low-energy (eV) electrons, keV ions and electrons, and MeV ions (see, e.g., reviews by Johnson and Quickenden, 1997; Delitsky and Lane, 1998; Johnson, 1990, 1998, 2001; Strazzulla, 1998; Baragiola, 2003; Johnson *et al.*, 2003). In spite of the considerable differences in excitation density and penetration depth for these incident particles, the results exhibit important similarities. Here we summarize the principal findings. We first note that the efficiency of this process in pure ice is likely to be lower than estimates based on very early measurements of the production of O_2 in ice (see, e.g., Hart and Platzman, 1961) because of low levels of contaminants in those early experiments (Baragiola and Bahr, 1998; Moore and Hudson, 2000). Therefore, trace species can be important in determining the O_2 production rates from Europa's icy surface and will be discussed shortly.

In studying the ability of energetic plasma particles to eject (sputter) molecules from ice, a process occurring on small Outer Solar System bodies, Brown, Lanzerotti, and co-workers (Brown

et al., 1982, 1984) found that, at temperatures relevant to the surface of Europa, H₂ and O₂ were important components of the ejecta. They then used those data to predict the presence of a radiolytically generated O₂ atmosphere on Europa (Johnson *et al.*, 1982). The production efficiency for gas-phase O₂ was found to be strongly temperature dependent, as seen in Fig. 2a for MeV He⁺ ions incident on ice and Fig. 2b for keV Ar⁺ ions on ice. In Fig. 2 the production rate is given as a yield, which is the number of molecules ejected per incident ion (i.e., O₂ production rate divided by the flux of incident particles: photons, electrons, or ions). Yields are typically measured at a low incident particle flux so that sample heating does not occur. The yield versus temperature shown in Fig. 2 appears to increase exponentially with *T* over a range of temperatures. Although this is not an Arrhenius dependence, rough activation energies can be extracted over narrow ranges of *T* (e.g., Fig. 2a, inset). These are of the order of 0.01–0.07 eV (Table 2). Such values are much smaller than those for diffusion of vacancies or trapped species in ice (Livingston *et al.*, 2002), but are comparable to the reported activation energies for H⁺ or H diffusion in ice, as noted earlier (Johnson and Quickenden, 1997). The lowest energies are also comparable to the enthalpy difference between amorphous solid water and crystalline ice (Ayotte *et al.*, 2001). Therefore, the estimated energies are likely

related to H⁺ and H transport or to hydrogen bond re-orientation. It has also been shown that as the temperature is increased above ~80–100K morphological changes occur that can affect the reaction kinetics and give incorrect activation energies. This is especially so when using measurements of average quantities, such as yields, rather than directly extracting rate constants by measuring transients (Selby, 2003). In addition, the activation energies can be representative of the competing (destruction) processes, rather than the formation processes (e.g., Matich *et al.*, 1993) as discussed in the model section.

The measured O₂ production rates (yields) were also found to be fluence dependent, where fluence is the radiation flux × the time or the total number of particles per unit area onto the ice. Multiplying the fluence by the incident particle energy and dividing by the average penetration depth gives the energy per unit volume, often called an average dose. As seen in Fig. 3, the O₂ yield versus fluence rises from zero, implying that a single ion incident on a fresh surface does not efficiently produce and eject oxygen. This is the case even for an incident 1.5 MeV Ne⁺ for which the excitation density along the ion path is high. However, it is seen in Fig. 3 that with increasing irradiation time individual impacting ions produce and eject O₂ with increasing efficiency as the material is chemically altered. At large fluences the yield appears to saturate, indi-

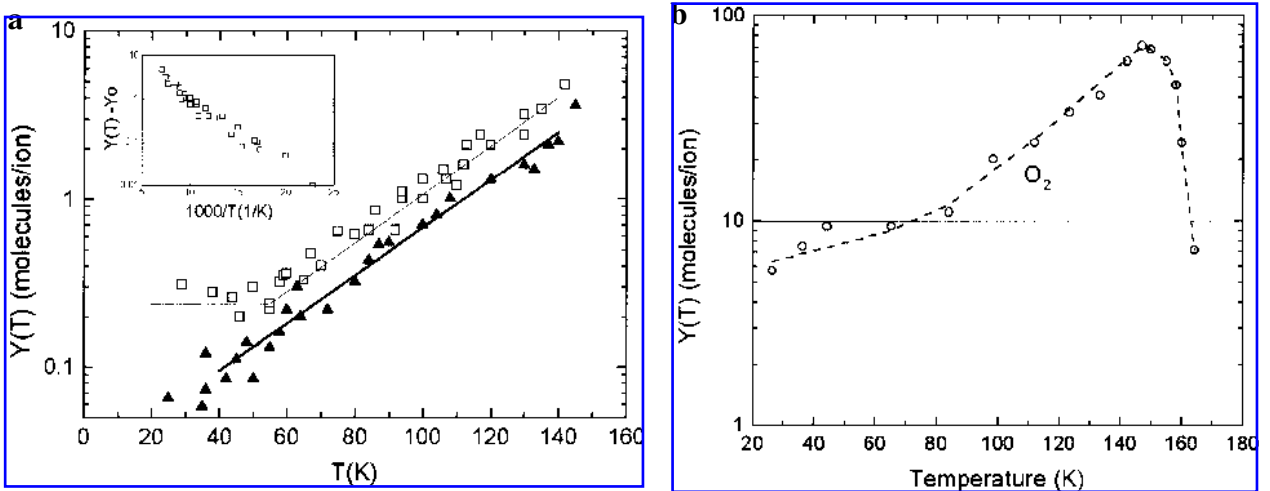


FIG. 2. a: Yield for D₂ and O₂ at saturation (steady state) from 1.5 MeV He⁺ on D₂O ice versus the temperature of the ice (adapted from Brown *et al.*, 1982). **Inset:** D₂ yield minus the constant yield at low *T* versus 1/*kT*, giving an average activation energy of 0.03 eV. b: Yield of O₂ at saturation versus temperature for incident 30 keV Ar⁺ ions (adapted from Baragiola *et al.*, 2003).

TABLE 2. OXYGEN AND PEROXIDE PRODUCTION

Radiation ^a	Product	T (K)	E _a (eV)	Percent at saturation	G (product/100 eV) ^b
He ⁺ (¹)	O ₂				0.15
γ(^{2,3})	O ₂	77 (300)			0.003 (0)
Ne ⁺ (30 MeV)(³)	O ₂	300			0.031
He ²⁺ (6 MeV)(³)	O ₂	300			0.008
He ²⁺ (29 MeV)(³)	O ₂	300			0.0016
H ⁺ (80 keV)(⁴)	O ₂	70			0.0002
H ⁺ (200 keV)(⁵)	O ₂	120			0.0007
He ²⁺ (1.5 MeV)(⁶)	O ₂	50 (100)	0.03		(0.7–4) × 10 ⁻⁴
Ne ⁺ (1.5 MeV) (⁷)	O ₂	7		10–15 ^c	0.03
(⁸)		70–140	0.05–0.07		0.1
Ar ⁺ (0.1 MeV)(⁹)	O ₂	30–140	<0.01–0.04		0.006–0.08
		160			0.01
e (30–100 eV)(¹⁰)	O ₂	120	0.02–0.03		0.005–0.007
hν (10.2 eV)(¹¹)	O ₂	50 (100)	0.03		0.0001 (0.0003)
H ⁺ (1 MeV)(¹²)	H ₂ O ₂	16 (77)			0.1 (<0.01)
+ 10% CO ₂		77			0.1
+ 10% O ₂		77			0.4
H ⁺ (30 keV)(¹³)	H ₂ O ₂	16 (77)		0.22 (0.38)	0.098 (0.086)
C ⁺ (30 keV)	H ₂ O ₂	16 (77)		1.7 (2.2)	0.23 (0.34)
N ⁺ (30 keV)	H ₂ O ₂	16 (77)		1.6 (1.4)	0.21 (0.11)
O ⁺ (30 keV)	H ₂ O ₂	16 (77)		1.4 (4.0)	0.26 (0.15)
Ar ⁺ (30 keV)	H ₂ O ₂	16 (77)		2.2 (2.0)	0.11 (0.06)

^aReferences are as follows: ¹Lefort (1995); ²Ghormley and Stewart (1956); ³Baverstock and Burns (1976); ⁴Baragiola *et al.* (1999); ⁵Baragiola and Bahr (1998); ⁶Brown *et al.* (1982) (ion does not stop in sample); ⁷Benit and Brown (1990) (ion does not stop in sample); ⁸Reimann *et al.* (1984) (ion does not stop in sample); ⁹Baragiola (2003); ¹⁰Sieger *et al.* (1998) (steady-state value); ¹¹Westley *et al.* (1995) (steady-state value as no fluence dependence seen); ¹²Moore and Hudson (2000); ¹³Gomis *et al.* (2003).

^bG values are for escaping O₂. For H₂O₂ and O₂ formation, both of which require multiple events, yields after saturation are used. In a few cases yields are obtained by melting the sample. Values in parentheses are those at another temperature.

^cPercent of film eroded as O₂ molecules for long-term irradiation.

cating that destruction processes are in a rough steady state with formation processes. The yields shown in Fig. 2 are purportedly those after saturation, although full saturation is often approached slowly.

The slope of the O₂ yield versus fluence, shown in Fig. 3, increases with increasing temperature, giving the activation energies in Table 2. These values are similar to those obtained from Fig. 2. For energetic ions that fully penetrate the film, as in Fig. 2a and 3a, the yield versus fluence can exhibit a second rise at higher fluences for which the radiation track cores begin to overlap. This increase also depends on temperature and exhibits similar activation energies (Reimann *et al.*, 1984). The strong dependence on temperature is at first surprising, since the energy density deposited by a 1.5 MeV Ne⁺ produces transient temperatures in the track core that are much higher than the ambient material temperature. Therefore, track temperature (local excitation density) alone does not determine the O₂ yield.

For all incident particle types and energies, the measured fluence dependence is found to be stable over laboratory time scales. That is, for experiments carried out at high vacuum, the yield returns to the value it had when the beam was turned off. This indicates that the irradiated ice is “permanently” altered (Reimann *et al.*, 1984). Thus a relatively stable chemical state is created that is favorable for O₂ production. This could be the formation of a particular trapped radiation product in ice that acts as a stable precursor or is due to the altered chemical and physical state of the irradiated ice. Trapped O, H₂O₂, and HO₂ (Matich *et al.*, 1993; Johnson and Quickenden, 1997; Sieger *et al.*, 1998) have been proposed as stable precursor species.

Using isotopically labeled H₂O, Benit and Brown (1990) showed that considerable transport of O occurs along the ion track when an energetic heavy ion penetrates an ice sample. Because of this, the O₂ yield was found to depend on sample thickness. Therefore, for thin ice samples the

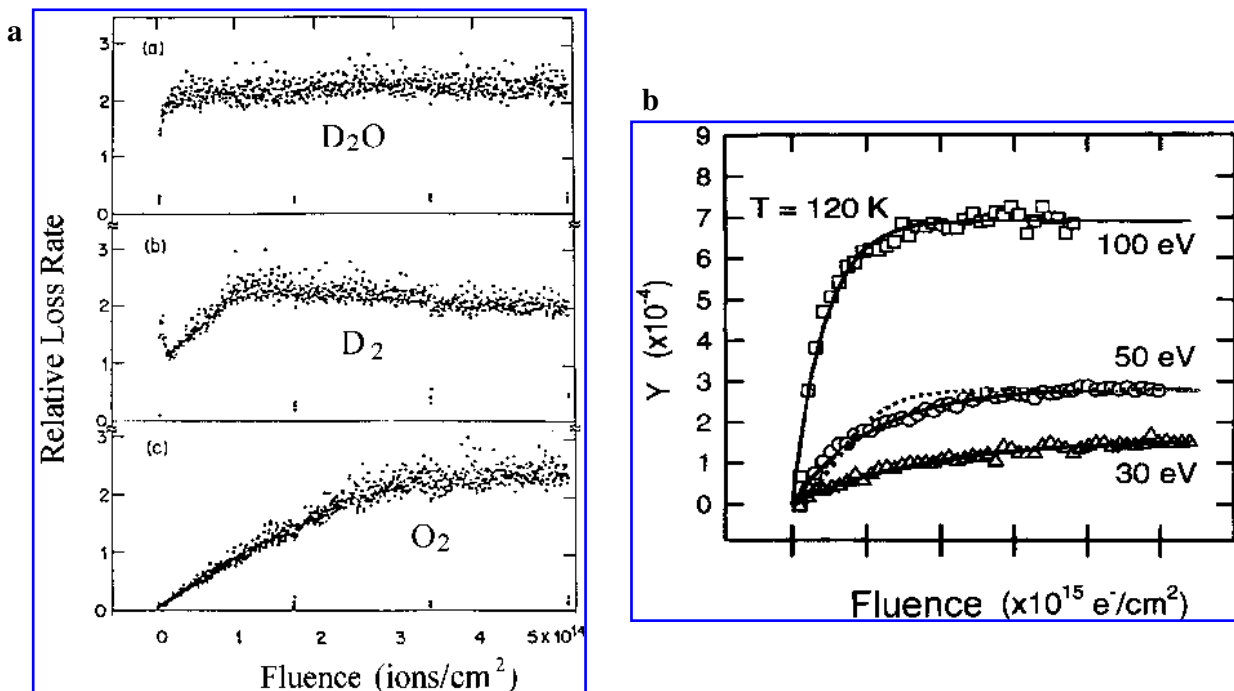


FIG. 3. **a:** Relative yields versus fluence (ion flux \times time) for 1.5 MeV Ne⁺ incident on D₂O ice at 7K (adapted from Reimann *et al.*, 1984). **Top panel:** D₂O yield. **Middle panel:** D₂ yield. **Bottom panel:** O₂ yield. Yields at other temperatures exhibited similar dependences with the slope of O₂ yield versus fluence varying with T . Fits give activation energies between ~ 0.02 eV at the lowest fluences and lowest T to ~ 0.07 eV at the highest T and highest fluences. **b:** Oxygen yield versus fluence of low-energy electrons on D₂O ice (from Sieger *et al.*, 1998).

“saturated” yields change slowly with fluence. More importantly, O from water molecules at a considerable depth into the sample contributed to the O₂ ejected from the surface. Since there was no observed diffusion of the O₂ in ice at the ambient temperature (7K) over the time for their experiment, they concluded that the oxygen transport and production are stimulated by the incident ions. The transport was suggested as being due to percolation/diffusion along the damaged and transiently heated tracks (Reimann *et al.*, 1984; Benit and Brown, 1990). They also found that in fully eroding (sputtering) thin ice films, the total amount of O₂ produced required about 10–15% of the D₂O molecules in the films at $T = 7$ K. On warming irradiated samples, some O₂ formed at depth is found to remain trapped for experimentally relevant times (see, e.g., Hart and Platzman, 1961; Benit and Brown, 1990; Baragiola and Bahr, 1998).

Matich *et al.* (1993) detected luminescence in 77K H₂O and D₂O ice from newly formed and excited O₂. They suggested that the O₂ is formed

from the interaction of a freshly produced, mobile O interacting with a previously produced and trapped O or H₂O₂. They favored the former. In matrix isolation studies of peroxide irradiated by UV photons luminescence from newly formed excited O₂ was seen. However, the oxygen was formed from mobile O (greater than ~ 30 K in Kr lattice) interacting with O trapped as H₂O-O (Khriachtchev *et al.*, 2000). These studies also suggest that trapped O, possibly in the form H₂O-O, may be an important precursor.

In Fig. 4a, the O₂ yield for low-energy electrons plotted as a function of electron energy exhibits an apparent “threshold” at ~ 10 eV (Orlando and Sieger, 2003). Although the uncertainties are large, the authors suggested there may be a lower threshold, ~ 6 eV, corresponding to a very small cross section for O₂ production ($\sim 10^{-20}$ cm²). This could be associated with an excitation at the ice surface. Bulk ice exhibits very weak absorption at photon energies below ~ 6 eV, but exhibits a strong absorption that, depending on the ice structure, begins at about 7.3 eV with a peak at ~ 8.6 eV. This

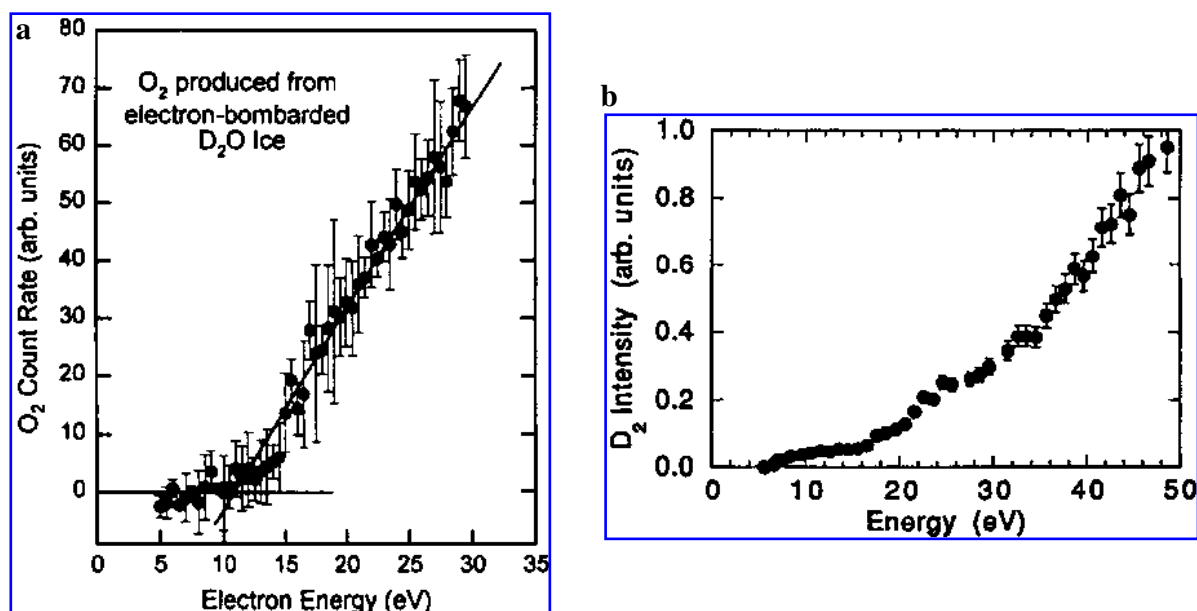


FIG. 4. a: Relative yield of O_2 from D_2O ice versus incident electron energy, E , at $T = 120K$ (from Orlando *et al.*, 1998; Orlando and Sieger, 2003). b: Relative yield of D_2 from D_2O ice versus incident energy, E , at $T = 88K$ (from Kimmel *et al.*, 1994).

is followed by a peak in absorption at ~ 10 eV. The results in Fig. 4a show that there is a dramatic increase in the production of O_2 at ~ 10 eV, which is the onset of secondary electron production in the bulk (Orlando and Sieger, 2003).

For incident fast ions, the yield at a given temperature was found, after a small fluence, to be independent of whether the sample was crystalline or amorphous ice (Brown *et al.*, 1982). However, using low-energy electrons the yields were found to be smaller for an initially crystalline ice (Orlando and Sieger, 2003). Since very low doses of ion radiation (a few eV per molecule) can convert crystalline ice to amorphous ice at low temperatures (Leto and Baratta, 2003), the damage produced by the penetrating ions used by Brown *et al.* (1982) affected the O_2 yield. The structural damage produced may create trapping sites, cause changes in the electronic relaxation pathways, or enhance percolation.

The temperature dependence of the O_2 yield is shown in Fig. 5 for electrons incident on initially amorphous (Fig. 5a) and initially crystalline (Fig. 5b) ice. A small decrease in efficiency is seen in both cases at ~ 120 – $130K$, where I_c forms from amorphous ice and pore collapse occurs (Rowland *et al.*, 1991). This is followed by an increasing yield with increasing T and then by a more

dramatic drop near $\sim 160K$ where I_h forms. During the transition to I_h trapped molecules have been shown to escape efficiently from ice samples (Ayotte *et al.*, 2001). A large drop in the yield is also seen in Fig. 2b for incident Ar^+ ions.

In modeling the dramatic decreases in the yield in Figs. 2b and 5 care must be taken. That is, the time for crystallization of an amorphous sample (Baragiola, 2003), even allowing for the large uncertainties, is <30 min at $\sim 145K$ and becomes <1 min at $160K$. Therefore, pulsed radiolysis experiments should be carried out at these temperatures, and the transients observed. Since the time for conversion from amorphous to crystalline ice can be shorter than the experimental times at $>145K$, the results are not comparable to those for which the chemical state of the ice at a given fluence is stable over experimental times. Below we focus on the data below $\sim 140K$.

We have emphasized processes initiated by the electronic excitations and ionizations produced. However, momentum transfer collisions, which are the dominant energy loss process for low-energy ions, also produce dissociations, defects, and O_2 in ice (Bar-Nun *et al.*, 1985). The relative efficiency of momentum transfer and electronic processes for producing O_2 needs further study. As the penetration depths are much smaller when

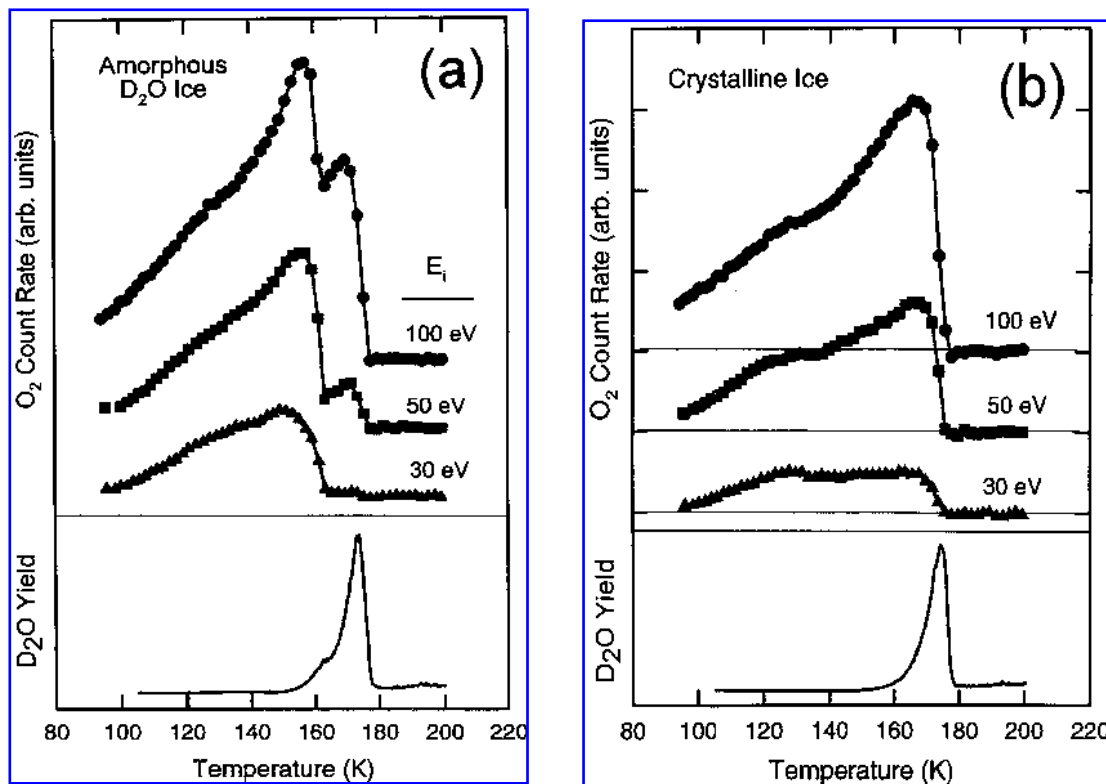


FIG. 5. a: Relative steady-state yields of O₂ from a D₂O ice sample versus T (**upper panel**). The ice samples were formed and irradiated at these temperatures. Film erosion as a yield (**lower panel**) (from Orlando and Sieger, 2003). b: Relative steady-state yields of O₂ versus T as in (a) (**upper panel**). Here the D₂O ice samples are formed at 160K, presumably becoming crystalline, and then irradiated at the T shown. A new sample is used for each data point in (a) and (b). Film erosion as a yield (**lower panel**) (from Orlando and Sieger, 2003).

the former dominates, the produced O₂ likely escapes readily.

H₂ formation and loss: correlation with O₂

The production of O₂ from a low temperature ice by radiolysis correlates with the formation and loss of H₂ (or D₂ from D₂O ice) (Reimann *et al.*, 1984). D₂O is used to reduce the background in mass spectrometry studies. The yields of O₂ from D₂O and H₂O ices were shown to be comparable. However, the total yields from D₂O were about 10% less (Reimann *et al.*, 1984), consistent with H (D) transport being important. It is seen in Fig. 3 that D₂ is promptly produced and lost from the D₂O ice. At higher fluence, the D₂ yield is seen to exhibit a dependence like that for O₂. For the 1.5 MeV Ne⁺ ions, which fully penetrate the ice sample, the D₂ yield eventually decreases since D₂ is produced and escapes from the full thickness of the film.

Because of H₂ (D₂) loss the surface region of

the irradiated ice becomes depleted in H (D) relative to O favoring the formation of oxygen-rich species. The change seen in the ratio of H (D) to O in the irradiated ice is small. An irradiated film (~100 nm) remains stoichiometric to better than 2% (Brown *et al.*, 1980) and in the near surface region Auger spectroscopy suggests only a slight oxygen enhancement due to irradiation by keV electrons (Rye *et al.*, 1978). Sieger *et al.* (1998) suggested a precursor concentration of the order of a percent. Such concentrations are an order of magnitude smaller than the steady-state concentration of dissociated H₂O (Table 2).

Using infrared spectroscopy the damaged H₂O concentrations at low temperatures in the saturation regime are about 10% over the irradiated volume (Benit *et al.*, 1987; Watanabe *et al.*, 2000; Gomis *et al.*, 2003). This fraction is the ratio of the dissociation cross section to the effective cross section for recombination to H₂O as discussed later. At a 10% concentration most H₂O will have a neighbor that is dissociated.

At temperatures above $\sim 40\text{K}$ it is seen in Fig. 2 that the D_2 and O_2 yields exhibit the same temperature dependence, suggesting a correlation between D_2 and O_2 loss. H_2 (D_2) can be formed by reactions between diffusing hydrogen from dissociated water or directly [i.e., $\text{H}_2\text{O}^* \rightarrow \text{H}_2 + \text{O}$ (e.g., Kimmel and Orlando, 1995); $\text{H}_2\text{O}^* \rightarrow (\text{H} + \text{OH})_{\text{cage}} \rightarrow \text{H}_2 + \text{O}$ (e.g., Matich *et al.*, 1993); $\text{H}_3\text{O}^+ + e \rightarrow \text{H}_2 + \text{OH}$ (e.g., Williams *et al.*, 1996)]. Subtraction of the nearly constant D_2 yield in Fig. 2a gives the Arrhenius plot in the inset. Since molecular hydrogen readily escapes at these temperature, it is the H_2 (D_2) formation process that has an activation energy of ~ 0.03 eV/molecule. The fact that slopes of the yields for H_2 and O_2 above $\sim 40\text{K}$ are similar suggests that H_2 (D_2) formation and loss is the rate-limiting step in determining the production and loss of O_2 at these temperatures.

Although the data at low T in Fig. 2a have considerable uncertainties, below about $20\text{--}40\text{K}$ the D_2 production is roughly independent of temperature, but the O_2 yield continues to decrease with decreasing temperature. Radiolytically produced D_2 is mobile and can escape above $\sim 15\text{--}20\text{K}$ (Watanabe *et al.*, 2000), but O_2 is immobile at such temperatures, and the incident He^+ ions are much less efficient at causing percolation than the incident Ne^+ discussed earlier.

The production of H_2 (D_2) from ice has also been studied using low-energy electrons and UV photons at very low temperatures. In the former studies, absolute yields were not obtained, but there appeared to be a threshold at ~ 6.3 eV (Fig. 4b). This is roughly the threshold for excitation of a surface state (Khusnatdinov and Petrenko, 1992), and the threshold for peroxide production is close to this value. The efficiency for H_2 (D_2) production increases around ~ 11 eV with a second steep rise at ~ 17 eV (Kimmel *et al.*, 1994). The O_2 and D_2 yields versus electron energy in Fig. 4 exhibit some similarity in the threshold region, although the uncertainties are large and the sample temperatures different. Measuring the H_2 (D_2) and the O_2 ejecta simultaneously over a range of temperatures, as in the Ne^+ experiments, would be instructive.

Using 9.8 eV photons at low T (12K) Watanabe *et al.* (2000) measured the D_2 ejected and trapped in ice. They obtained a cross section for production of D_2 (Table 2) at low fluences that is $\sim 10\text{--}20\%$ of the total absorption cross section with significant uncertainties. They also found

that the equilibrium damage fraction in the sample was $\sim 10\text{--}20\%$ of the D_2O molecules, but the equilibrium production of D_2 was about an order of magnitude smaller, $\sim 1\text{--}2\%$ at their temperatures. They suggested that the D_2 is formed at grain interfaces and cracks and on the surfaces of pores. In a mixed ice, $\text{D}_2\text{O} + \text{CO}$, exposed to UV photolysis, D_2 and CO_2 formation are correlated (Watanabe and Kouchi, 2002). The D_2O dissociates to produce D_2 plus O , and this transiently mobile O reacts with CO to produce CO_2 .

Precursor state and peroxide

In order to produce O_2 from low temperature ice, it appears that the ice sample must lose hydrogen and form trapped, oxygen-rich, reactive species. The efficiency of production also appears to be affected by the level of defects and damage in the ice, consistent with the suggestion that the hydrogen-bonding network is important in the production of O_2 via availability of trapping sites, new electronic relaxation pathways, or the nature of the bonding of precursors. Here we briefly examine the possible role of the suggested precursor molecules H_2O_2 and HO_2 . We note that H_2O_2 might not readily dissolve in ice, possibly accounting for its low abundance in some experiments. It appears to be heterogeneously distributed in the form of microcrystals (Gurman *et al.*, 1967). If H_2O_2 does act as a precursor, the formation of aggregates could affect the dimer absorption bands (Cooper *et al.*, 2003a) and affect the production and stability of O_2 (Cooper *et al.*, 2003b).

The results of Gerakines *et al.* (1996), in which ice at $\sim 10\text{K}$ is irradiated by UV photons, confirm that H_2O_2 forms in ice from two OH after a build-up of trapped OH . They monitored the band associated with $\text{H}_2\text{O}\text{--}\text{HO}$ (Langford *et al.*, 2000), in which the HO is bound to water with ~ 0.24 eV. Therefore, they might only be monitoring a subset of the trapped OH seen in earlier experiments (e.g., Taub and Eiben, 1968). The H_2O_2 concentration in ice reaches a steady-state level at fluences of about 10^{18} photons/ cm^2 (Gerakines *et al.*, 1996). As seen in the model section, this gives an estimate of the H_2O_2 photodestruction cross section of the order of 10^{-18} cm^2 . Similarly, HO_2 begins to be seen in absorption at about a few times $10^{17}/\text{cm}^2$ shortly after they begin to detect H_2O_2 . The absolute yields were not measured.

Westley *et al.* (1995) detected H_2 and O_2 pro-

duced by Lyman- α (9.8 eV) radiation of ice, but found no fluence dependence for fluences greater than $\sim 10^{17}/\text{cm}^2$. They also saw small amounts of H_2O_2 by programmed thermal desorption of the sample, but made no quantitative evaluation. Comparing their lowest fluence for the production of O_2 with the result of Gerakines *et al.* (1996) for peroxide suggests that H_2O_2 and HO_2 are probably not important precursors of O_2 . In UV photolysis of H_2O_2 using 6.4 eV photons the production of O_2 was not observed (Vaghjiani *et al.*, 1992), and the excitation of an irradiated ice, which presumably contained some peroxide, by 3.7 eV photons did not produce O_2 (Baragiola *et al.*, 2003). Direct excitation of matrix-isolated H_2O_2 at low temperature also did not yield O_2 , but the production of a mobile O that reacted with trapped O ($\text{H}_2\text{O}-\text{O}$) did give O_2 (Khriachtchev *et al.*, 2000).

Irradiating with 200 keV protons at temperatures of 40–129K, Bahr *et al.* (2001) found only about 0.001–0.02% H_2O_2 using programmed thermal desorption as compared with earlier experiments that suggested larger values (e.g., Table 2). Using infrared absorption Moore and Hudson (2000) found a G value of ~ 0.1 for incident MeV protons at low temperature, but the signal in the observed band became negligible at 80K, suggesting that H_2O_2 was not being formed. They also found that adding O_2 significantly increased the production efficiency of H_2O_2 . That is, that the amount of peroxide was affected by the amount of trapped oxygen. Based on the matrix isolation studies (Khriachtchev *et al.*, 2000), dissociated mobile O might trap as $\text{H}_2\text{O}-\text{O}$, which on excitation converts to H_2O_2 . Therefore, even if H_2O_2 is not the precursor, the peroxide and trapped oxygen concentrations will be related.

Although molecular oxygen was not a product of photolysis of matrix isolated H_2O_2 , it was a product of photolysis at 266 nm (4.66 eV) of peroxide dimers in an argon matrix: $2 \text{H}_2\text{O}_2 \rightarrow 2 \text{H}_2\text{O} + \text{O}_2$ (Engdahl and Nelander, 2002). This decomposition was thought to be due to the considerable distortion of the bonds in the dimer. Therefore, the configuration or distortion by the lattice of peroxide or any other precursor molecule in the ice may be critical (Sieger *et al.*, 1998). In addition, more recent experiments show that G values for the production of H_2O_2 by 30 keV incident ions are significant, as are the steady-state ratios of $\text{H}_2\text{O}_2/\text{H}_2\text{O}$ (Gomis *et al.*, 2004). Ratios of the order of 0.2–4% were found at 16K and

77K in the irradiated regions, with incident H giving the smallest fraction and incident O the largest (Table 2). At these concentrations, peroxide molecules might segregate, forming inclusions (Gurman *et al.*, 1967; Cooper *et al.*, 2003b). Since the amount of trapped peroxide also competes with the amount of trapped O, studies are needed to describe the chemical state of the solid produced by radiolysis. This will be critical in describing the fate of the irradiation products at Europa. In particular, the chemical composition favorable for producing O_2 needs to be determined, as does the importance of trapped O, H_2O_2 , HO_2 , or peroxide dimers as precursors.

Other species

In the model below, we will refer to atomic and molecular species trapped in ice. Such species are often discussed in the literature on radiolysis and photolysis (for summaries, see Matich *et al.*, 1993; Johnson and Quickenden, 1997). Trapped OH, O, H_2O_2 , and HO_2 have been discussed and/or measured by a variety of techniques (absorption and luminescence spectroscopy, electron spin resonance, programmed thermal desorption, etc.). Care must be taken when using these data as results for ice samples formed below $\sim 160\text{K}$ or those exposed to penetrating ion beams likely have numerous defects, voids, and grain interfaces so that a variety of trapping sites and trap depths exist. Therefore, when a particular band for a trapped species (e.g., OH) disappears with increasing temperature, it could be due to a change in the nature of the trapping as well as to loss of the species by reaction.

Although H is discussed below, we do not distinguish it, in these simple models, from H^+ trapped as the hydronium ion, H_3O^+ , which would mean that there are corresponding negative ions present. Therefore, below we refer to the various species as if they are neutral, although this might not be the case. Although trapped electrons are detected only over a narrow range of temperatures (~ 100 – 120K), negative ions must be important over a broad range of temperature.

We also note that SO_2 and a sulfate, and CO_2 and a carbonate, appear to be trapped species in Europa's icy surface. Under radiolysis each of these can dissociate directly, giving O_2 . However, with the exception of the sulfate, their densities are less than 1%, so they are not relevant sources of O_2 . However, their presence is indicative of the

preference for forming oxygen-rich molecules in Europa's ice and can affect the efficiency of production of O₂ and H₂O₂.

MODELS FOR FORMATION OF O₂

Introduction

Based on the data described above, the yields for incident electrons and ions are found to be nearly linear in fluence at the lowest fluences for which O₂ is detected. In addition, the relevant alterations of the ice samples by radiolysis appear to be stable and independent of the beam flux. Remarkably, this is the case both for low-energy electrons that make only a single excitation for each impact and fast ions that make a density of excitations along their path through the solid. This suggests that O₂ is produced and trapped in the initial events and then caused to escape from the solid by the subsequent radiation, or that a stable chemical alteration of the ice is required before the radiation can produce and eject O₂.

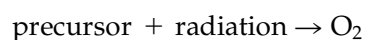
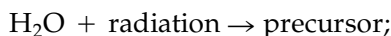
Because H produced by the dissociation of water molecules can attack trapped O₂ and any precursor oxidants, the loss of H is important. This occurs by the production and loss of hydrogen molecules, as discussed, leaving a surface that is slightly rich in O relative to H. The O₂ production mechanism could be direct excitation of a particular precursor species, or it might not be specific. That is, a new OH or O produced by the incident radiation could react with the H-depleted solid, producing O₂. This would occur more efficiently as the ratio of O to H in the near surface region increased.

In their early work, W.L. Brown and colleagues assumed that processes similar to those used to describe radiolysis of liquid and gaseous H₂O could be used to describe the radiolysis in ice. The low activation energy that they found was assumed to be associated with diffusion of some mobile radical species in ice, such as H or O, or, possibly, diffusion of the O₂ molecule itself. Based on their studies of ejection from isotopically labeled D₂O samples, they concluded that the O₂ is formed in the track of a single ion and then ejected by subsequent ions (e.g., Benit and Brown, 1990). More recently, trapped species have been suggested as precursors. These are either subsequently excited by the incident radiation or attacked by newly produced mobile

species. We consider a simple model that incorporates all of these processes and can be used to organize and interpret the experimental data. We also discuss its relationship to more complete models. In this discussion, much of which is in the Appendix, we consider the standard radiation products that have been often described. However, in a solid, the excited electron cloud produced by absorption can overlap a number of lattice sites. Therefore, their relaxation pathways and/or product species could be very different from those that have been traditionally considered in the literature on radiolysis and photolysis.

Precursor model

The column density of a precursor species, N_p , formed in ice by incident radiation can be calculated using a simple model. In this model cross sections are used for the production, σ_p , and destruction, σ , of the precursor. O₂ is then formed by excitation of the precursor or by reaction of a newly formed radical with the precursor. This is also described using a cross section, σ_{O_2} . For incident electrons having a small penetration depth, the O₂ produced is assumed to rapidly diffuse to the surface and escape (Sieger *et al.*, 1998). More generally, we define N as the column density of H₂O from which the incident radiation can produce and eject O₂. A pair of rate equations gives both N_p and the production rate of oxygen, dN_{O_2}/dt . That is,



giving

$$dN_p/dt = \sigma_p \phi N - \sigma \phi N_p \quad (1)$$

$$dN_{O_2}/dt = \sigma_{O_2} \phi N_p \quad (2)$$

In Eq. 1 ϕ is the incident flux, and the total precursor *destruction* cross section can be written as $\sigma = \sigma_p' + \sigma_{O_2}$, with σ_p' accounting for precursor destruction processes other than the formation of O₂. Solving Eqs. 1 and 2, and assuming N is nearly constant ($\sim 10\%$ level as discussed), the fraction of precursors, c_p , in the affected column after time t is obtained (Appendix):

$$c_p = N_p/N = [\sigma_p/\sigma] [1 - \exp(-\sigma \Phi)] \quad (3)$$

Here $\Phi = [\phi t]$ is the fluence (flux \times time), which

is the number of particles (photons, electrons, or ions) incident on the surface per unit area. Using c_p in Eq. 2, the O_2 yield, Y , at any fluence can be written in terms of the yield at steady state, Y_∞ :

$$Y = [dN_{O_2}/dt]/\phi = \sigma_{O_2} c_p N = Y_\infty [1 - \exp(-\sigma\Phi)] \quad (4a)$$

$$Y_\infty = [\sigma_p \sigma_{O_2} / \sigma] N \quad (4b)$$

If we also account for the reduction in the density of water molecules in the initial column N , these forms change only slightly. The size of the two parameters Y_∞ and σ can be obtained by fitting the yield versus fluence data, such as that in Fig. 3.

For the low-energy electron data, Sieger *et al.* (1998) showed that the ratio, $[Y/Y_\infty]$, for a given incident electron energy is independent of temperature over a narrow range of temperature. Therefore, the destruction cross section, σ , in Eq. 4a is roughly independent of T and can be estimated from the $[Y/Y_\infty]$ curve. Sieger *et al.* (1998) found a precursor destruction cross section $\sigma \approx 0.8\text{--}3.0 \times 10^{-16} \text{ cm}^2$ for incident electron energies from 30 to 100 eV. This is of the order of the electron impact ionization cross section for H_2O .

Based on the above model, the lack of an observed fluence dependence for fluences down to $\sim 10^{17} \text{ hv/cm}^2$ in the Lyman- α irradiation of ice (Westley *et al.*, 1995) can be examined. The lowest fluence used implies that the precursor destruction cross section for Lyman- α is of the order of the Lyman- α absorption cross section in ice ($\sim 0.9 \times 10^{-17} \text{ cm}^2$).

Sieger *et al.* (1998) also assumed that $\sigma_p' = 0$. This would mean that the precursor is only destroyed by production of O_2 (i.e., $\sigma = \sigma_{O_2}$). That is unlikely since suggested precursors can be destroyed by reaction with H and other radicals. Their assumption would also mean that the cross section for production of O_2 from a precursor, σ_{O_2} , is large. This would be surprising and appear to contradict some of the data discussed above. Instead, we assume that σ is not equal to σ_{O_2} and the total destruction cross section, σ , is of the order of the ionization or absorption cross section.

Having obtained σ , the measured temperature dependence for production of O_2 is contained only in Y_∞ . Over a narrow range of T , one can write $Y_\infty(T) \approx Y_\infty' \exp(-E_a/kT)$ and obtain the es-

timate of the activation energies in Table 2. If $\sigma_p' \neq 0$, as discussed, then σ_p and σ_{O_2} in Eq. 4b cannot be obtained separately from the data for Y_∞ unless an independent measure of c_p is obtained. Such a measurement is critical for describing the chemical state of the irradiated surfaces.

The observed temperature dependence of Y_∞ is contained in σ_p , σ_{O_2} , or N . Here N is the "depth" from which newly formed O_2 can reach the surface and escape given as a column density of H_2O . The physical depth is obtained by dividing the column density N by the molecular number density of the ice. Assuming that in the low-energy electron experiments N is independent of temperature and is about three monolayers (Sieger *et al.*, 1998), the measured Y_∞ gives $[\sigma_{O_2}\sigma_p/\sigma] \sim 0.5\text{--}2.0 \times 10^{-18} \text{ cm}^2$ over the electron impact energy range. At 110–120K, this ratio was found to be proportional to $(E - E_0)$ for $E > E_0 \sim 10 \text{ eV}$, again assuming fixed N (Orlando *et al.*, 1998; Orlando and Sieger, 2003).

In the following section we first consider a precursor, like peroxide, that typically forms from two dissociation events. We use this to show under what circumstances such a model does not violate the observed linearity of the O_2 yield data with fluence. Following that, we relate the simple precursor model above to the case where trapped O is the precursor. We then use the model for trapped O to examine the effect of the trap density on the production of O_2 . The density of traps (defects) is determined by the sample formation temperature and the subsequent radiation damage. Finally, we consider the escape depth, N , for penetrating radiation within the precursor model. These discussions are supported by more detailed rate equations in the Appendix.

Precursor: trapped peroxide

The proposed precursor peroxide is typically formed from products of two dissociation events: i.e., $2 H_2O \rightarrow 2 H + 2 OH \rightarrow H_2 + H_2O_2$. This was confirmed in low temperature ice (Gerakines *et al.*, 1996). It is also possible that a dissociation producing a trapped O, followed by an excitation event, can produce peroxide: $2 (H_2O + hv) \rightarrow H_2 + H_2O\text{-O} + hv \rightarrow H_2O_2 + H_2$ (e.g., Khriachtchev *et al.*, 2000). The O_2 yield versus fluence for incident electrons is reasonably well fit by the yield expression above for fluences greater than $\sim 10^{14} / \text{cm}^2$. Therefore, it has been suggested that

any precursor species must be formed in a single event. Using a model in the Appendix in which the precursor is formed by two events, we show this is not necessarily the case. Precursor formation, if it is fast, could involve two dissociation events and give the measured fluence dependence. Although we consider peroxide here, these conclusions apply to other possible precursors.

In the example in the Appendix, H_2O is dissociated to $\text{H} + \text{OH}$ according to the cross section σ_d . The reactions of two OH units to form H_2O_2 (rate constant, $k_{2\text{OH}}$) and 2 H to form H_2 ($k_{2\text{H}}$) compete with the recombination of H and OH to H_2O ($k_{\text{H,OH}}$). If $k_{2\text{H}}$ is much greater than $k_{2\text{OH}}$, then H_2 loss dominates at low fluences as expected (Appendix). Steady state requires, not surprisingly, that the rate for forming H_2O_2 is roughly equal to the rate for forming H_2 . Finally, it is seen in the Appendix that the low H_2O_2 concentrations suggested by experiment imply that $k_{\text{H,OH}} \gg (k_{2\text{H}} k_{2\text{OH}})^{0.5}$. Such sizes are reasonable.

The set of rate equations in the Appendix that use number densities of species is integrated over depth in order to obtain the forms used in Eqs. 1 and 2, which are based on column densities. In this way the effective cross sections are related to the rate constants for the interaction of freshly produced mobile species with previously produced trapped species. We show in the Appendix that the O_2 yield versus fluence can be written in a form similar to that in Eq. 4a but with a small offset due to the two-step precursor formation process:

$$Y \approx Y_\infty(T) [1 - \exp(-\sigma\Phi) - (\sigma/\sigma_r)];$$

$$\text{for } \Phi \gg \sigma_r^{-1} \quad (4c)$$

Here σ is again the precursor destruction cross section, but $\sigma_r = (2\sigma_{2\text{OH}} + \sigma_{\text{H,OH}})$ is the effective cross section for loss of OH by formation of H_2O_2 and H_2O . The corresponding expression for $Y_\infty(T)$ is given in the Appendix.

The form for the yield versus fluence in Eq. 4c is consistent with the low-energy electron measurements if $(\sigma/\sigma_r) \ll 1$ and if $\sigma_r \gg \Phi^{-1} \approx 10^{-14} \text{ cm}^2$. Such sizes are indeed possible. What is required is that, at the relevant temperatures (50–110K), the interaction length associated with σ_r is more than a few molecular layers (greater than $\sim 10 \text{ \AA}$). A cross section that is likely to be large above $\sim 20\text{K}$ is $\sigma_{\text{H,OH}}$, which describes the mean distance for diffusion of mobile H before it

reacts. Since σ , discussed earlier, is of the same order of magnitude as the H_2O dissociation cross section, σ_d , then the precursor concentration, c_p , (in this case H_2O_2) is roughly proportional to $[\sigma_{2\text{OH}}/\sigma_{\text{H,OH}}] \ll 1$ (Appendix).

Based on the above, a two-step precursor formation process could be consistent with the electron data, contrary to the statements in Sieger *et al.* (1998), Orlando *et al.* (1998), and Orlando and Sieger (2003). Experiments are needed to determine the relevant cross sections. Below we consider a precursor formed in a single excitation event.

Precursor: trapped O

O_2 can be formed, for instance, by diffusion of a transiently mobile O to a previously formed and trapped O or to the production of O near the site of a previously produced and trapped O (Matich *et al.*, 1993; Johnson and Quickenden, 1997). We refer to this as the Matich–Johnson–Quickenden (MJQ) model and note that $\text{O} + \text{OH} \rightarrow \text{O}_2 + \text{H}$ can also give molecular oxygen.

Trapped O as $\text{H}_2\text{O-O}$ was in fact seen to be a precursor to O_2 when attacked by a mobile O in a Kr matrix (Khriachtchev *et al.*, 2000). Therefore, O trapped as $\text{H}_2\text{O-O}$ was also suggested as a precursor in ice (Johnson, 2001). Before proceeding we note that the examination of the MJQ model in Sieger *et al.* (1998) was incorrect. They considered two mobile interacting species whose lifetimes were long compared with the bombardment rate, rather than a new mobile O interacting with a previously trapped O. Although this has not been corrected, recently they added O trapped as $\text{H}_2\text{O-O}$ as a possible precursor (Orlando and Sieger, 2003). O trapped as $\text{H}_2\text{O-O}$ is seen in matrix isolation studies, as discussed above, but it has not yet been identified in ice, and, like OH, it may trap in a number of ways.

The MJQ model is essentially the following. Formation of $\text{H}_2 + \text{O}$ is followed by loss of H_2 and trapping of O (O_t). A subsequent dissociation or excitation event can lead to the destruction of O_t by reaction with, for instance, H or by conversion to H_2O_2 . However, if this dissociation event also leads to $\text{H}_2 + \text{O}$, a mobile O is produced that can react with O_t with an interaction length that depends on T . This results in the formation of O_2 [$\text{O} + \text{O}_t \rightarrow \text{O}_2$] giving a net production of 2 H_2 and 1 O_2 . In the Appendix the relevant rate equations (Eqs. A1c–A3c) are con-

sidered. Assuming the mobile O processes are fast, these rate equations can also be integrated and simplified to give the form in Eqs. 1 and 2. The precursor column density, N_p , now represents the column density of O_t . In this model, σ_{O_2} in Eq. 2 is the "cross section" for reaction of a freshly produced O with an O_t , and σ_p' indicates destruction of O_t . Finally, σ_p is the cross section for production of H_2 and O_t via processes discussed above.

Based on the sizes of the cross sections extracted in the electron irradiation experiments, the model with trapped O (O_t) as the precursor is quantitatively reasonable. That is, for a range of T , both σ_p and σ_{O_2} might be described by events of the type $H_2O \rightarrow H_2 + O$ (whether direct or indirect). If these occur for $\sim 10\%$ of the radiation-induced dissociation events as discussed, then the required product of cross sections suggested by the sizes of σ and Y_∞ above is roughly obtained: that is, $[\sigma_p \sigma_{O_2}] \sim 0.2\text{--}6 \times 10^{-34} \text{ cm}^2$ in the low-energy electron experiments. The cross section for production of O might depend on the availability of dangling bonds at interfaces, in pores, or at defects, as suggested by a number of authors. The importance of such bonds could also be consistent with the differences in the electron-induced yield for initially crystalline and initially amorphous ice (Orlando and Sieger, 2003).

O_2 production can increase in the presence of oxygen-rich impurities, such as CO_2 or SO_2 , both of which are known to be present at Europa. As in the MJQ model, dissociation (e.g., $CO_2 \rightarrow CO + O$) can provide a mobile O that can be trapped or react with a previously trapped O, forming O_2 . In addition, such species are hydrogen scavengers (Moore and Hudson, 2000). This can reduce the destruction of O_t affecting σ_p , as seen in Eq. A5c.

Trap density

In the simplified models above, the density of trapping sites, n_t , was not explicitly accounted for. However, in the discussion of both the experimental data and models, trapping sites have been assumed to be important. It has been demonstrated repeatedly that the density of defects, voids, and interfaces decreases as the temperature of formation of the ice increases. However, the efficiency of production of O_2 is the opposite; it increases with increasing T . Therefore, the oxygen yield varies in a manner that is

the inverse of the trap density over a range of temperatures. For penetrating ions in which the energy density deposited is high and O_2 might be formed in a single track, a simple explanation has been given. As the density of traps for O_2 is reduced and the temperature increases, the O_2 produced can diffuse to the surface and escape more efficiently, limiting back reactions on further irradiation. This is examined in the next section. However, such a process does not affect the low-energy electron yields for which the penetration depth is small and the formed O_2 escapes readily at the measurement temperatures. In Eqs. A1c, A1c', A3c, and A10 in the Appendix, we again use a simple set of rate equations for trapped and mobile O in order to determine the role of the trap density, n_t , on the production of a precursor species. The conclusions apply to any model based on a trapped precursor.

In the MQJ model, mobile O can be trapped forming O_t (described by $k_{O,t} n_t$) and can react with previously trapped O to form O_2 (k_{O,O_t}). In addition, it can react at other sites, and O_t can be destroyed by mobile reactive species such as H ($k_{H,O_t} n_H$). Mobile H can also react with other trapped species ($k_{H,R} n_R$). Incorporating these reactions, Eq. A10 in the Appendix gives a steady-state yield, Y_∞ . When the density of traps is large, the steady-state yield is given in Eq. A5c:

$$Y_\infty \rightarrow (\sigma_d' \sigma_d / \sigma_d) \{ [k_{O,O_t} k_{H,R} n_t] / [k_{H,O_t} k_{O,t} n_t] \} N \quad (5)$$

Here σ_d and σ_d' are the dissociation cross sections that determine the production of H ($H + OH$) and O ($H_2 + O$) by the incident radiation. Comparing the result in Eq. 5 with Y_∞ in the simple precursor model in Eq. 4b, the dissociation cross sections in Eq. 5 are now scaled by a ratio of the reaction rates.

It is seen in Eq. 5 that the steady-state yield, Y_∞ , depends inversely on the density of traps, n_t . That is, there are competing destruction processes for trapped O (O_t). Therefore, in order to form O_2 a mobile O competes with mobile H to find a trapped O before it becomes trapped. In this way, the increasing O_2 yield correlates with the reduction in the trapping sites with increasing temperature of formation. The small activation energies discussed earlier would be related to the re-orientation of the lattice binding leading to the reduction in trap density. At relatively high T the density of traps becomes small, so that only the

sample surface or grain interfaces might act as traps, accounting for the observed drop in the yield at high T . For this reason, it is important to determine if the yield for T greater than $\sim 150\text{K}$ depends on the incident flux, ϕ . Since other quantities in the expression for Y_∞ could also be temperature dependent, experiments are needed. These would likely be pulsed radiolysis experiments in which the transients are studied rather than the steady-state yields. However, the available data for lightly ionizing radiation do suggest that the O_2 yield depends inversely on trap density, as in the model above.

Escape from depth

The quantity N in Eq. 1 is the "depth" given as a molecular column density from which O_2 formed below the surface can percolate to the surface and escape. It can be converted to a physical depth by dividing by the molecular number density of the ice. In the case of the low-energy electrons, the depth below the surface at which ionizations and excitations are produced is small. However, for fast ions that penetrate many monolayers, this is not the case. Below we examine N in Eq. 1.

Although it has long been understood that two excitations events are required to produce O_2 (e.g., Brown *et al.*, 1982; Reimann *et al.*, 1984), the precursor model suggests that at saturation (steady state) any new event can produce O_2 from the steady-state density of trapped precursors. Therefore, one might expect the yield at saturation to be nearly linear in the excitation cross section. This is the case for the low-energy electrons, and it was initially assumed to be the case for the fast ions (Brown *et al.*, 1980; Reimann *et al.*, 1984). However, Baragiola *et al.* (2003) showed that the total sputtering yield in the saturation region at temperatures greater than $\sim 100\text{K}$, which is dominated by decomposition (Brown *et al.*, 1982), is proportional to the square of the electronic energy deposition per unit path length in the solid, $(dE/dx)_e$. Assuming that the production and destruction cross sections in Y_∞ in Eq. 4b roughly scale with $(dE/dx)_e$, then their ratio $[\sigma_p \sigma_{\text{O}_2}/\sigma]$ also roughly varies as $(dE/dx)_e$. If this is the case, then the observed quadratic dependence implies that the depth, N , from which O_2 can be mobilized to escape, must also depend on the excitation density, $(dE/dx)_e$. This is consistent with the observation that the O_2 yield depends on thickness for samples thinner than the ion penetration

depth (Reimann *et al.*, 1984; Benit and Brown, 1990). Therefore, the percolation depth for escape, N , is a critical factor in comparing yields for penetrating radiation with those for non-penetrating radiation, like the low-energy electron and low-energy ion data. It is also seen that percolation and trapping can be included within the simple model considered here.

Model summary

We have examined the simple precursor model introduced by Sieger *et al.* (1998) to explain their electron data. We have shown how it can be generalized and derived from an integration of the appropriate chemical rate equations, with the cross sections and total column density containing the reaction rates and the physics of diffusive transport. Therefore, the parameters can have very different meanings from those initially assumed. The equations are useful when there are fast processes, which go to completion in times much shorter than the time between particle impacts, and slow processes, associated with species that are assumed to be trapped between particle impacts. This separation allowed us to examine those models proposed for precursor formation and destruction due to reacting mobile species formed from dissociation events. Further, from the size of the onset of the linearity of the yield versus fluence we can place constraints on the role of nonlinear processes, such as those that might be associated with the formation of a precursor like peroxide.

With these extensions, this simple model is useful for approximating the full rate equations in the temperature region for which the yields depend on the fluence (dose) and not on the dose rate. Based on the assumptions in the model, this implies temperatures at which precursor species are stable over experimental times. At the highest temperatures for the yields shown in Fig. 4a, this might not be the case. This should be tested experimentally. In this regard, it is puzzling that experiments have shown that the absorption bands associated with certain trapped species, such as OH and trapped electrons, "disappear" at $\sim 100\text{--}120\text{K}$ (see, e.g., Johnson and Quickenden, 1997), whereas the O_2 yield data indicate that relevant precursor species must be stable to $\sim 140\text{K}$. Therefore, the proposed O_2 production processes can only be distinguished by directly determining the chemical state of the irradiated ice.

It may be the case that a particular precursor is not required, as mentioned earlier. Rather, after a sufficient level of oxidation a newly produced O or OH can react in the oxygen-rich lattice producing O₂ in a pseudo-first-order process. This can be tested experimentally. Indeed, trapped O and peroxide may be changed into one another as in the matrix isolation experiments (Khriachtchev *et al.*, 2000). Therefore, their relative concentrations versus temperature and dose should be studied.

In the model considered here, it is seen that the parameters in Y_{∞} must account for the strong temperature dependence. Since the number of bulk trapping sites decreases with increasing T as the ice sample is annealed, one might expect that the precursor concentration would decrease. We suggest that the observed temperature dependence is determined by the competition between the availability of trapping sites and mean interaction distances of a mobile species such as O and H. That is, the O₂ yield varies inversely with the density of traps over a range of temperatures. In the simple model above, this effect is included indirectly as shown using the more detailed equations in the Appendix.

EUROPA

Oxygen and peroxide production at Europa: G values

The dependence of the yield on the thickness of the ice sample for highly penetrating ions suggests that the O₂ yield is roughly related to the amount of energy deposited in the sample. Therefore, the amount of O₂ produced and lost from ice in steady state is often given as a G value, the number of molecules produced per 100 eV deposited in Table 2. In applying these G values to the planetary environment care must be taken, since the yields are temperature, fluence, and excitation density dependent. They also are affected by the presence of other proton scavengers known to be present in Europa's ice.

The G values for peroxide in Table 2 are those for production at low fluence, but the G values for O₂ are for the production and escape of gas-phase oxygen at saturation. Therefore they depend on the formation and destruction cross sections in the model above. Such G values can be used to describe the steady-state source of the am-

bient O₂ atmosphere at Europa, but are not helpful in determining the ability to produce and trap O₂ at depth into the icy surface. Over the time scales of the experiments, some O₂ is seen to remain trapped and is not destroyed by radicals. Typically, there are a number of trapping sites, and recent estimates of the activation energy for an O₂ molecule trapped in a substitutional site (Hori and Hondoh, 2002) suggest that it can be trapped for times comparable to the time required for the conversion of amorphous ice into Ih (Ayotte *et al.*, 2001). The stability of O₂ inclusions has not been studied.

To understand the relationship between the G values for O₂ in Table 2 we note that fast light ions and electrons lose their energy predominantly by producing ionizations and excitations. The ionization events produce secondary electrons that can result in further ionizations. The number of ionization events, N_i , produced by a fast light ion stopping in a water ice is, $N_i = E_0/W$, where E_0 is the initial energy and W is the average energy expended per ionization event, ~ 27 eV in water ice. Therefore, radiolysis by fast ions is often described as the net effect of the shower of electrons set in motion by the incident ion. In this manner, the G values for production of O₂ from ice by energetic light ions and electrons can be roughly estimated as the sum of the effects of all the secondary electrons using the yield, Y_e , for ~ 10 – 100 eV electrons. That is, if we ignore the percolation depth, N , we can write the number of O₂ produced as the number of ionization events times Y_e , which already has in it the destruction processes. That is, $G \sim N_i Y_e / E_0 \sim Y_e / W \sim 0.006$ O₂/100 eV.

This estimate of G is seen to be an order of magnitude larger than the keV proton value for O₂ in Table 2 but is much smaller than the G value for energetic Ne⁺. These differences from the simple estimate are consistent with the observation that the yield in the saturation regime for penetrating ions varies nonlinearly with excitation density. The difference from the keV proton G value is likely due to the inability of O₂ to escape from depth before destruction. On the other hand, the larger G value seen using MeV Ne⁺ is likely due to the high density of excitation. This can result in more efficient production of O₂, increased production of damage sites for forming O₂, and/or increased transport (percolation) along the transiently heated track. That is, the ability of the formed O₂ to percolate to the surface during ion

bombardment plays an essential role in determining the measured yields as discussed above. This effect needs to be evaluated for a planetary surface subject to particle fluxes that are many orders of magnitude smaller than those used in the laboratory.

In the absence of O₂ yields for all of the relevant ions and energies, an estimate of the total supply of O₂ can be obtained using the *G* values in Table 2. For the energetic oxygen and sulfur ions we use *G* values for neon and argon ions. These are lower bounds as the data were obtained at temperatures much lower than the surface temperatures at Europa (80–110K). For the fast, penetrating electrons and protons, we use the value for 200 keV protons in Table 2. For the heavy ions we used the Ne⁺ and Ar⁺ values. For comparison we also give an estimate using the *G* values obtained from the low energy electron data and the total ionization, as discussed above.

The *G* values are combined in Table 3 with the electron and ion energy flux at Europa. Although there is some deflection of the flow due to induced fields, the net energy flux to the surface is not reduced much from these values (Paranicas *et al.*, 2002). In fact, locally produced pick-up ions, which are formed from the ejecta and accelerated to the surface, can contribute (Ip, 1996). Further, although *G* values are typically independent of the incident angle, the loss of O₂ is a surface process and is enhanced with angle. That is, the number of O₂ produced within the escape depth increases with increasing angle to the normal (steeper than the inverse cosine). This enhancement is ~2.5–4 (Jurac *et al.*, 2001). Ignoring such corrections, the total production rate calculated

(2.3–6.2 × 10⁹ O₂/cm²/s) is a lower bound to the actual production rate from the icy regions of Europa's surface. Recent modeling of the O₂ atmosphere suggest that such a source rate is required (Shematovich and Johnson, 2001).

Earlier estimates of the O₂ source rate were incorrect because O₂ production was assumed to be a fixed fraction of the H₂O sputtering yield. At the ambient temperature an ejected H₂O sticks efficiently (Smith and Kay, 1997) to the surface of neighboring grains in the porous regolith, reducing the sputtering yield for H₂O (Johnson, 1989). This reduction does not apply to the O₂ fraction of the yield, enhancing its relative importance to H₂O. Here we assume that all of the gas-phase O₂ produced can contribute to the ambient atmosphere, even if it is produced at a grain surface that is at some depth into the porous regolith.

Finally, Europa's surface is not pure ice everywhere. That is, much of the trailing hemisphere is a hydrated sulfuric acid containing small amounts of sulfur and SO₂, and the leading hemisphere contains low levels of carbon, CO₂, and carbonates. Sodium and potassium atoms are sputtered from the icy regions (e.g., Leblanc *et al.*, 2002). O₂ production from surfaces containing these species has not been measured. C and S are both proton scavengers, and the other species can be sources of O as discussed, so that the O₂ yield from such regions could be enhanced. However, there can also be competing processes that might reduce these rates. In fact, recent HST observations suggest that the O₂ might not be produced uniformly across Europa's surface (McGrath *et al.*, 2000). The analysis of these observations is preliminary and is not simple since the observed

TABLE 3. APPLICATION TO EUROPA

Species	Implantation 10 ⁹ /cm ² s ^a	Energy flux 10 ⁹ keV/cm ² s ⁽¹⁾	Oxygen production 10 ⁹ /cm ² s
H (>10 keV)	0.015 ⁽¹⁾	12	0.084 (0.72) ^b
O (>10 keV)	0.015 ⁽¹⁾	1.8	>0.54 ^c
S (>10 keV)	0.009 ⁽¹⁾	3.0	>0.90 ^c
Electrons		62	0.43 (3.7) ^b
Plasma (<~10 keV) (13.7 amu)	~1.3 ⁽²⁾	1.0	>0.3 ^c
Total		79	>2.3 (6.2)
UV photons (>6.4 eV)		46	<0.1

^aReferences are as follows: ¹Cooper *et al.* (2001) [similar results in Paranicas *et al.* (2002)]; ²Mauk *et al.* (1996).

^bUsing *G* for 200 keV protons (upper bounds in brackets are based on the low-energy electrons data as a model for the secondary electrons produced).

^cUsing *G* for 1.5 MeV Ne⁺ at 7K, a rough lower bound.

emissions depend on the local plasma properties. However, the efficiency of O₂ production in contaminated ices needs to be studied.

Porous regolith: O₂ interactions on grain surfaces

Although the O₂ atmosphere is principally produced in the near surface layers and is eventually lost to space, it also permeates Europa's porous regolith. The porosity, p (void space), of the regolith is uncertain (Buratti, 1995). It has been estimated to be the most compact surface in the Outer Solar System, $p \sim 0.25$ on the trailing hemisphere and $p \sim 0.79$ on the leading hemisphere (Buratti and Veverka, 1983), and the most porous surface, $p \sim 0.96$ globally (Domingue *et al.*, 1991; Domingue and Hapke, 1992). These large differences are due to the uncertainties in the amount of backscattered light at small phase angles and on the photon absorption properties and grain sizes. The more compact surface is likely correct. Grain sizes, r_g , of the order of 100 μm have been suggested (Hansen and McCord, 1999, 2000; Geissler *et al.*, 1998). Europa's regolith differs significantly from the lunar regolith, which is a sand-like surface of individual grains. Analysis of the thermal inertia of Europa's surface (Grundy *et al.*, 2001) suggests that the ice grains are sintered, forming a fairy castle-like structure. Sintering can occur thermally or due to the incident radiation. In addition, ices doped with acids and alkalis in the laboratory can be powdery solids with the impurities primarily found at grain interfaces.

The porous regolith affects the above estimates of the oxygen production in three ways. First, for isotropic bombardment the mean distance, d , into the surface at which an incident ion or photon strikes a grain surface is $d \sim (8/9)r_g/(1-p)$. Using the above value for r_g , then $d \sim 0.2$ m if the porosity is very large: $p \sim 96\%$. Therefore, desorbed molecules can come from a considerable depth and will interact with grain surfaces. Even for much lower porosities the effective sputtering yields can be significantly modified (Johnson, 1989). As discussed above, the yields for ejected H₂O, which sticks onto neighboring grains at the ambient temperatures, are reduced, but those for ejected O₂ are not. This enhances the relative importance of the O₂ yields.

Finally, the surfaces and interfaces of the sintered grains in Europa's porous surface are places where low temperature chemistry involving the

ambient oxygen can occur at depths that are well below the nominal penetration depth of the incident radiation. The relative importance of such chemistry is roughly indicated by the ratio of the total surface area in the regolith to the area of Europa's visible surface. Using the porosity and grain size above and a regolith depth, d_r , of the order of a meter, then this ratio is large: $\sim 3(1-p)d_r/r_g$, which is $\sim 10^3$ – 2×10^4 for average porosities of 96% and 25%, respectively. Therefore, the gas-phase O₂ molecules below the visible surface interact frequently with the grain surfaces. In this way a very large volume of the subsurface could be altered chemically even if it is not directly exposed to the radiation.

From the overlying structures seen in the high-resolution images of Europa's surface by the Galileo spacecraft (e.g., Prockter and Pappalardo, 2000), it is clear that the youngest surfaces are redder. The reddening in the visible has been attributed to the presence of sulfur in the ice (McEwen, 1986; Johnson *et al.*, 1988; Calvin *et al.*, 1995; Carlson *et al.*, 1999b). The amount of reddening in the spectra of the surface material decreases with age, and the surface materials appear to become brighter with age. This might occur by the slow accumulation of a frost over-layer or by radiolysis (Carlson *et al.*, 2002; Johnson *et al.*, 2003). Radiolysis preferentially converts the sulfur in the ice to sulfur dioxide or sulfuric acid, both of which have flat spectra in the visible. In regions where the radiation does not directly penetrate, the O₂ permeating the regolith can oxidize the sulfur at the surfaces of the icy grains and at grain interfaces. Similarly, the carbon seen in the ice on Europa's leading hemisphere (e.g., Carlson *et al.*, 2004; Johnson *et al.*, 2003) can be oxidized by radiolysis in the near surface layers or by reactions on the grain surfaces at depth in the regolith by the ambient O₂. The meteoroid bombardment that produces the regolith also exposes fresh surfaces for oxidation and can cause the collapse of pores, leading to the trapping of oxygen. In this manner, both refractory and volatile oxidants can be formed and trapped in the subsurface ice for potential delivery to Europa's subsurface ocean.

SUMMARY

The presence of a thin oxygen atmosphere and oxidants trapped in Europa's surface ice (e.g., Johnson *et al.*, 2003), combined with the possible

presence of a subsurface ocean (e.g., Carr *et al.*, 1998), have made Europa an exciting target for future space exploration. The molecular oxidants produced by radiolysis and photolysis could be species needed for carbon-based biochemistry in Europa's putative subsurface ocean. However, there has been no model for the formation, trapping, and transport of relevant oxidants.

In this paper we have reviewed the space observations and laboratory studies related to the chemistry of formation of oxidants in ice by the incident radiation. Because the laboratory data are incomplete, we examined the rate equations for formation of oxygen and related species by radiolysis and photolysis. We showed how such equations can be simplified to the analytic model that was used for fitting the fluence and temperature dependence of the O₂ yield produced by low-energy electrons (Sieger *et al.*, 1998). In deriving the analytic model from the more complete rate equations, the competition between formation and destruction processes can be studied, as can the role of trapping sites, escape from depth, and temperature history. These equations also allowed us to put incident photon, electron, and ion data on a similar footing for the first time.

The model can be used to suggest measurements that are needed to describe the chemical state of the irradiated ice and to interpret new laboratory data. We showed that if reactions are fast, the yield data could be consistent with a precursor being formed by two events, as is the case for peroxide. However, we favor trapped O as a precursor, as initially suggested by Matich *et al.* (1993) for production of excited O₂. Such a species, if present, could be detected spectroscopically, as can trapped O₂ through bands activated by lattice perturbations (Cooper *et al.*, 2003a).

The available oxygen yield data were used to compare *G* values for different incident particles. These were then used to estimate the oxygen production in the radiation environment at Europa. The lower bounds were consistent with the production rates obtained from a recent model of Europa's atmosphere. The porosity of the regolith was also considered. It not only affects the relative sputtering yields for O₂ and H₂O, but also provides an enormously increased surface area on which the ambient gas-phase oxygen can react with species in the ice. That this might be occurring is consistent with the change in re-

flectance associated with surface aging. Such reactions could also convert ambient molecular oxygen into other more refractory species that remain trapped on subduction of Europa's crust.

Although radiolysis produces a stable, chemically altered surface in the laboratory, the particle flux to Europa's surface is many orders of magnitude lower. Therefore, annealing can be effective at temperatures that are much lower than those typically found experimentally. Below about 120K the annealing times appear to be long (e.g., Baragiola, 2003) so that laboratory data can often be directly applied to Europa's icy surface. However, account has to be taken of the synergism between the UV and the energetic plasma, as discussed earlier (Johnson and Quickenden, 1997).

Transient surface melting might initiate life processes, but subduction of oxidants to the putative ocean is likely to be required if biochemistry is to occur at Europa (Chyba and Hand, 2001). Although the temperature versus depth into Europa's regolith is not well known, below the regolith the temperature and pressure apparently increase with depth. At some depth (approximately kilometers) either very warm ice or an ocean exists (Ruiz and Tejero, 2000). Therefore, chemically refractory oxidants are likely to be required in order to survive subduction to the warmer subsurface regions. Trapped species, if delivered downward, can become mobile and will segregate forming inclusions (Johnson and Jesser, 1997). Indeed, peroxide appears to segregate in ice (Gurman *et al.*, 1967), and these inclusions may remain relatively stable until the peroxide is dissolved in the putative ocean. The volatiles seen in reflectance, such as O₂, SO₂, and CO₂, will also segregate. But at the higher temperatures they could also diffuse through the bulk, react, or percolate into the regolith atmosphere. Therefore, the observation of the trapped volatiles in Europa's surface ice is of interest primarily because it suggests that oxidants are present. The formation of oxygen-rich molecules follows the preferential loss of hydrogen. However, the surface is in a local steady state with implanted H, O, and S from the plasma and the loss to space. Since the plasma flux to the surface can be variable, this balance can also vary. Indeed temporal changes in reflectance have been reported (Domingue and Hendrix, 2004).

Based on the models for formation of O₂ ex-

amined in this paper, additional experiments are needed to determine the chemical state of irradiated ice at low fluences. Of immediate interest is the identification of stable molecular precursors required for the formation of O_2 . Based on the available laboratory data, individual peroxide molecules trapped in the ice do not appear to be the principal precursors, but trapped O (Matich *et al.*, 1993) remains a viable candidate. Although the data suggest that the local hydrogen-bonding network is important in the production of O_2 , the effect of the formation temperature and radiation damage on the structure need to be measured. It is also important to describe quantitatively the relationship between H_2 loss and the formation of O_2 and H_2O_2 over a range of temperatures and fluences. Finally, one would like to determine the steady-state densities of biochemically interesting molecules formed by radiolysis in an ice containing sulfur and carbon at Europa's surface temperatures, and then determine their stability with increasing temperature and pressure. Such experiments still need to be carried out. Here we have presented a model that brings together the various laboratory data and now can be used to consider the formation trapping and transport of relevant oxidants at Europa.

APPENDIX

Introduction

In this Appendix we examine rate equations that describe various aspects of the radiolysis or photolysis of ice. These equations need to be understood if one is to be able to calculate the formation, trapping, and transport of oxidants. The emphasis is on the formation of molecular oxygen. We integrate these equations over the escape depth of O_2 to give the simplified rate equations discussed in the text in which number densities are replaced by column densities (e.g., Eqs. 1 and 2). In this way we can examine the relationship between the rate constants and the effective precursor formation and destruction cross sections extracted from data. We first consider a precursor, such as H_2O_2 , that is formed from two excitation events. This bears on the observed linearity of the oxygen yield versus fluence. We then consider the equations for trapped versus a tran-

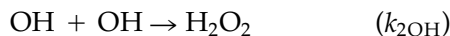
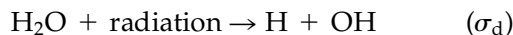
siently mobile species. We use a reaction between a mobile and trapped O as an example, although $O + OH$ can also give oxygen. Finally, we examine the possible dependence of the O_2 formation process on the density of traps (defects, voids, and grain boundaries) as a function of temperature. The results are discussed in the text.

For clarity, all possible radiolytic species are not included in the discussion below. Therefore, potentially important products such as HO_2 and the charged species (e.g., H_3O^+ , the trapped electron, etc.) are missing. In each section we attempt to make a point related to production of O_2 and other oxidants by using a subset of the products rather than attempt a complete description with many unknown rate constants.

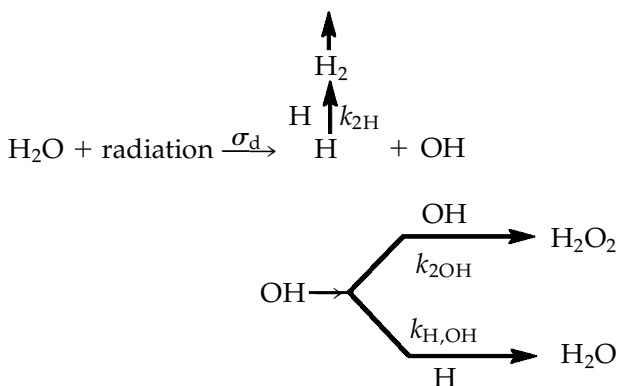
Fast versus slow processes

To describe the O_2 production rate from a precursor such as H_2O_2 , we first use a simple but instructive set of rate equations to describe the formation of H_2O_2 . We then relate these to the simplified rate equation for the precursor in the text, Eq. 1, and show how the postulated precursor formation cross section, σ_p , is related to the H_2O dissociation cross section, σ_d , by the reaction rates.

Using the reactions:



the reaction pathways are described by:



The corresponding rate equations in an irradiated volume are

$$dn_{\text{OH}}/dt = \sigma_d \phi n - 2 k_{2\text{OH}} n_{\text{OH}} n_{\text{OH}} - k_{\text{H,OH}} n_{\text{H}} n_{\text{OH}} \quad (\text{A1a})$$

$$dn_{\text{H}}/dt = \sigma_d \phi n - 2 k_{2\text{H}} n_{\text{H}} n_{\text{H}} - k_{\text{H,OH}} n_{\text{H}} n_{\text{OH}} \quad (\text{A2a})$$

$$dn_{\text{H}_2\text{O}_2}/dt = k_{2\text{OH}} n_{\text{OH}} n_{\text{OH}} - \text{destruction processes} \quad (\text{A3a})$$

Here σ_d is the dissociation cross section, ϕ is the radiation flux, and n is the molecular number density of ice, with n_{OH} and n_{H} the density of dissociation products OH and H, respectively. The rate constants $k_{2\text{OH}}$, $k_{2\text{H}}$, and $k_{\text{H,OH}}$ describe the reactions above. In this model, the H_2 formed is assumed to escape for temperatures above about 20K. We do not distinguish between trapped species and mobile species, although in fact that distinction is important as discussed in the next section. That is, any OH produced at low temperature by one ion would likely be trapped prior to interacting with an OH produced by a subsequent ion. At higher temperatures this can break down, as discussed in the text. We first relate the above set of equations to Eq. 1 in the text and then consider precursor destruction processes.

Equation 1 in the text is obtained by solving these equations together and then by integrating over a depth Δx . Here Δx is the smaller of the penetration depth of the particle and the O_2 escape (percolation) depth. Assuming the molecular density of ice, n , is constant with depth, $\Delta x n = N$ in Eq. 1. Comparing Eq. 1 with Eq. A3a, the precursor formation rate, $\sigma_p \phi N$, is equivalent to $[k_{2\text{OH}} n_{\text{OH}} n_{\text{OH}}] \Delta x$. Assuming that the processes in Eqs. A1a and A2a are fast, then the steady state is readily obtained. In addition, if $k_{2\text{H}} \gg k_{2\text{OH}}$, there is preferential loss of H_2 at short times as suggested by the laboratory data. If steady state is reached the production of H_2 is equal to that of H_2O_2 using only the equations above. Further, one obtains

$$[k_{2\text{OH}} n_{\text{OH}} n_{\text{OH}}] \Delta x \rightarrow [f_p \sigma_d] \phi N \quad (\text{A4})$$

with

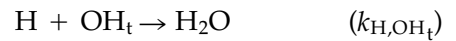
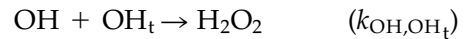
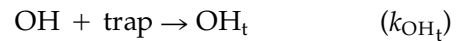
$$f_p = 0.5/[1 + 0.5 k_{\text{H,OH}}/(k_{2\text{H}} k_{2\text{OH}})^{0.5}] \quad (\text{A5a})$$

Therefore, the precursor formation cross section, σ_p , in Eq. 1 is a fraction, f_p , of the total dissociation

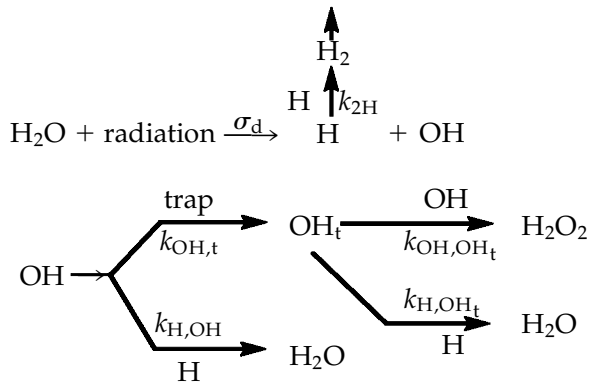
cross, σ_d . Since laboratory data suggest the H_2O_2 fraction in an irradiated ice is small, then $k_{\text{H,OH}} \gg (k_{2\text{OH}} k_{2\text{H}})^{0.5}$, which is likely, giving $f_p \rightarrow [(k_{2\text{OH}} k_{2\text{H}})^{0.5}/k_{\text{H,OH}}]$.

Trapped versus mobile species

To examine the fluence dependence discussed in the text we note that trapped OH and freshly produced, transiently mobile OH can be treated as different species (e.g., Matich *et al.*, 1993). Therefore, assuming no trapping of H, the OH rate equation above would be replaced by two equations: one for the trapped species, n_{OH_t} , and the other for the freshly produced mobile species, n_{OH} . Assuming the reaction of two mobile OH units is unlikely and that peroxide is formed from the interaction of a trapped OH with a subsequently produced OH, an expanded set of equations is obtained:



then the reaction pathways are described by



The resulting set of equations is:

$$dn_{\text{OH}}/dt = \sigma_d \phi n - k_{\text{H,OH}} n_{\text{H}} n_{\text{OH}} - k_{\text{OH}_t} n_{\text{OH}} n_t - k_{\text{OH,OH}_t} n_{\text{OH}} n_{\text{OH}_t} \quad (\text{A1b})$$

$$dn_{\text{OH}_t}/dt = k_{\text{OH}_t} n_{\text{OH}} n_t - k_{\text{OH,OH}_t} n_{\text{OH}} n_{\text{OH}_t} - k_{\text{H,OH}_t} n_{\text{H}} n_{\text{OH}_t} \quad (\text{A1b}')$$

$$dn_{\text{H}}/dt = \sigma_d \phi n - 2 k_{2\text{H}} n_{\text{H}} n_{\text{H}} - k_{\text{H,OH}} n_{\text{H}} n_{\text{OH}} - k_{\text{H,OH}_t} n_{\text{H}} n_{\text{OH}_t} \quad (\text{A2b})$$

$$dn_{\text{H}_2\text{O}_2}/dt = k_{\text{OH,OH}_t} n_{\text{OH}} n_{\text{OH}_t} - \text{destruction processes} \quad (\text{A3b})$$

where n_t is the trap density in the irradiated ice. At low T we can assume n_t is large so that $dn_t/dt \sim 0$, simplifying the set of equations. If the precursor of interest is trapped O, as discussed in the text, then a similar set of equations can be constructed for O and O_t as in the example to follow. Of course, a full description over a broad range of temperatures would require the consideration of the both trapped and mobile H, O, and OH, the rate of change of trap density, and the various destruction processes.

The above equations should be solved simultaneously, but, for the incident particle fluxes typically used in these studies, the diffusion of mobile species to traps is relatively fast. This is true even at low temperatures if there is a significant density of trapping sites. This is usually the case for samples formed at low T . Therefore, in a low temperature solid at low dose rates there is not a significant steady-state background of diffusing OH. There are trapped or freshly produced OH units, which rapidly react. Averaging over the bombardment rate this can be approximated by writing $dn_{\text{OH}}/dt \sim 0$ and then separating n_{OH} out in Eq. A1b. Assuming also that H diffuses rapidly and either reacts or forms H_2 we also write $dn_{\text{H}}/dt \sim 0$ on the average. Therefore, between impacts only species trapped at defects, pores, or grain surfaces are assumed to be present, as suggested by the lack of a dependence on the incident beam flux. In this limit the rate of change of trapped OH roughly simplifies to:

$$dn_{\text{OH}_t}/dt = 2 k_{2\text{H}} n_{\text{H}} n_{\text{H}} - 2 k_{\text{OH,OH}_t} n_{\text{OH}} n_{\text{OH}_t}$$

It is seen that the production of peroxide depends on the loss of H by formation of H_2 , as discussed, and at steady state the production rate for peroxide equals the rate of formation of H_2 in these equations.

Treating the mobile and trapped species separately, we can further simplify the rate equations and obtain the precursor model used in the text. That is, integrating over the relevant depth, Δx , the densities are replaced by column densities. The rate constants, k_i , are then related to effective cross sections, σ_i . In this way cross sections are given as an interaction length for each freshly produced mobile radical: $[k_i n_i] \rightarrow [\sigma_i \phi]$. The

trapped OH column density, N_{OH_t} , and peroxide production rate can be estimated from "linear" rate equations:

$$dN_{\text{OH}_t}/dt \approx [\sigma_d \phi] N - 2 [\sigma_{2\text{OH}} \phi] N_{\text{OH}_t} - [\sigma_{\text{H,OH}} \phi] N_{\text{OH}_t} \quad (\text{A6a})$$

$$dN_{\text{H}_2\text{O}_2}/dt \approx [\sigma_{2\text{OH}} \phi] N_{\text{OH}_t} - \sigma N_{\text{H}_2\text{O}_2} \quad (\text{A6b})$$

Here σ_d is again the dissociation cross section, and the destruction processes in Eq. A3b are contained in σ . The second and third terms on the right in Eq. A6a are the loss of OH due to the production of H_2O_2 and H_2O : In the integration of Eq. A1b' $[2 k_{\text{OH,OH}_t} n_{\text{OH}}]$ becomes $[2 \sigma_{2\text{OH}} \phi]$, and $[k_{\text{H,OH}_t} n_{\text{OH}}]$ becomes $[\sigma_{\text{H,OH}} \phi]$. Therefore, the density and the interaction length of mobile H are contained in $\sigma_{\text{H,OH}}$. If H_2O_2 is indeed the precursor, then in Eq. 2 in the text $[\sigma_p \phi N]$ becomes $[\sigma_{2\text{OH}} \phi N_{\text{OH}_t}]$ from Eq. A6b. Accounting for precursor destruction, which can give back two OH, and treating H_2 can both be included in the integrated model via the σ_i values.

The simplified set of equations above allows us to examine the relative time (fluence) scales for precursor formation (in this case H_2O_2). Solving Eqs. A6a and A6b, the column density of OH and the concentration of precursors versus fluence, c_p , can be obtained. Using the column of H_2O_2 produced as the precursor column, N_p , in Eq. 2, then O_2 yield can be obtained. The results can be compared with the results from Eqs. 1 and 2 in the text. The average precursor (H_2O_2) concentration over the column depth of water molecules, N , is:

$$c_p = f_p (\sigma_d/\sigma) \{ [1 - \exp(-\sigma \Phi)] - (\sigma/\sigma_r) [1 - \exp(-\sigma_r \Phi)] \} \quad (\text{A7})$$

with

$$f_p = 2\sigma_{2\text{OH}}/(\sigma_r - \sigma) \quad (\text{A5b})$$

In these equations, $\sigma_r = (2\sigma_{2\text{OH}} + \sigma_{\text{H,OH}})$ and $\sigma/\sigma_r < 1$.

It is seen that the precursor concentration with time, c_p , depends on two rates, the reaction rates that determine σ_r and the destruction rates in σ . As in Eq. 4a the yield can be written as:

$$Y = \sigma_{\text{O}_2} c_p N \quad (\text{A8})$$

If σ_r and σ are comparable, then the yield at small

fluence is quadratic in Φ . However, if $\sigma_t \gg \sigma$ then the linear dependence on fluence is obtained with a small shift in the fluence, as shown in Eq. 4c in the text. Further, the steady-state yield is now:

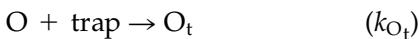
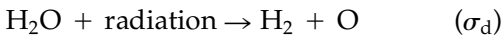
$$Y_\infty(T) = \sigma_{O_2} [f_p \sigma_d] N / \sigma \quad (\text{A9})$$

That is, $\sigma_p \rightarrow [f_p \sigma_d]$ as in Eq. A4, and the temperature dependence for the incident electron data must be contained in $[\sigma_{O_2} f_p]$ or in the ratio $[\sigma_{O_2} \sigma_{2OH}] / \sigma_{H,OH}$.

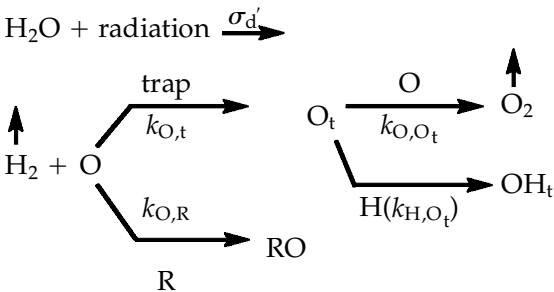
For comparison with their precursor model, Sieger *et al.* (1998) examined the possibility of obtaining the O_2 precursor by considering reactions for a density of diffusing dissociation products, as in Eqs. A1 and A2, rather than a trapped product interacting with a freshly formed dissociation product. Based on the above, the lowest fluence at which O_2 is first detected experimentally sets a limit on the time scale for mobile-mobile reactions.

Effect of trap density

Equations A1b, A1b', A2b, and A3b can be approximately solved assuming that the dn_{OH}/dt , dn_H/dt , and dn_t/dt are very small on the average as discussed above. In order to examine the role of the trap density, n_t , which can depend on the temperature and method of formation, and on the radiation history of the ice, we use the slightly simpler precursor model. In this model the O produced directly by dissociation traps forming a precursor. O_2 is then formed when a freshly produced O or other species reacts with a trapped oxygen atom, O_t :



The reaction pathways for the oxygen species are:



We assume, for simplicity, both H_2 and O_2 escape from depth Δx after formation. We also allow mobile H to react with O_t (k_{H,O_t}), removing trapped O and both the mobile H and O to be removed by other reactants, R (e.g., OH or contaminants). This leads to a simplified set of equations not directly involving OH or peroxide:

$$\begin{aligned} dn_O/dt = \sigma_d' \phi n - k_{O,t} n_O n_t - k_{O,R} n_O n_R \\ - k_{O,O_t} n_O n_{O_t} \quad (\text{A1c}) \end{aligned}$$

$$\begin{aligned} dn_{O_t}/dt = k_{O,t} n_t n_O - k_{O,O_t} n_O n_{O_t} \\ - k_{H,O_t} n_H n_{O_t} \quad (\text{A1c}') \end{aligned}$$

$$\begin{aligned} dn_H/dt = \sigma_d \phi n - k_{H,O_t} n_H n_{O_t} \\ - k_{H,R} n_H n_R \quad (\text{A2c}) \end{aligned}$$

$$dn_{O_2}/dt = k_{O,O_t} n_O n_{O_t} \quad (\text{A3c})$$

These equations, of course, act in parallel with the equations above for OH, and mobile OH may react with trapped O to form O_2 . Here we focus only on mobile O.

Since the diffusion of H and O are fast and the density of traps is large, the n_H and n_t averaged over the bombardment rate can be taken, very roughly, as time independent. Further, if we assume the number of trapped O, n_{O_t} , is small compared with the number of sites at which H can react, then $n_H \sim [\sigma_d \phi n / k_{H,R} n_R]$. For a low radiation flux, ϕ , n_H is small, on the average, as assumed. Since the O_2 yield, Y_{O_2} , is equal to $[(dn_{O_2}/dt) \Delta x / \phi]$ with Δx the escape depth, then the steady-state yield, Y_∞ , can be obtained analytically:

$$\begin{aligned} [Y_\infty] / [\sigma_d' N] = 1 + \{(q - 1) - [(q - 1)^2 \\ + 8 q \delta]^{0.5}\} / 4 \delta \quad (\text{A10}) \end{aligned}$$

$$q = [k_{O,t} (n_t + n_R)] (k_{H,O_t} n_H) / (\sigma_d' \phi n) k_{O,O_t}$$

$$= (\sigma_d / \sigma_d') [k_{O,t} (n_t + n_R)] k_{H,O_t} / [k_{O,O_t} k_{H,R} n_R]$$

$$\delta = 0.5 [1 + n_t / (n_t + n_R)]$$

We note that for n_t large, q can be large. Assuming that $q \gg 1$ and $n_t \gg n_R$ then Eq. A10 becomes:

$$Y_\infty \rightarrow [\sigma_d' N] / q = (\sigma_d' N) (\sigma_d' / \sigma_d)$$

$$[k_{O,O_t} k_{H,R} n_R] / [k_{H,O_t} k_{O,t} n_t] \quad (\text{A5c})$$

Comparing with Y_∞ in the simple precursor model in Eq. 4b, then $\sigma \rightarrow [(k_{H,O_t} n_H)/\phi] \rightarrow [\sigma_d n_{k_{H,O_t}}]/[k_{H,R} n_R]$. In addition, the product $[\sigma_{O_2} \sigma_p] \rightarrow \{\sigma_d' \sigma_d' [k_{O,O_t} n]/[k_{O,t} n_t]\}$. That is, the dissociation cross sections are modified by reaction rates.

Quite remarkably, it is seen in Eq. A5c that the steady-state yield, Y_∞ , can depend inversely on the density of traps, n_t , in the temperature and flux regimes for which the approximations are relevant. That is, if there are competing destruction process for trapped O, then at high trap density a mobile O must find a trapped O before it becomes trapped or before mobile H destroys the O_t . In this way the increasing O_2 yield with increasing T can be related to the change in the trapping density, n_t , with the formation temperature of the ice sample. As the temperature increases and the density of traps in the bulk decreases, the surface and grain interfaces become the only trapping sites.

ACKNOWLEDGMENTS

R.E.J. acknowledges support by a Gladden Fellowship in Chemistry, School of Biomedical and Chemical Sciences at The University of Western Australia, and by grants from the NSF Astronomy Program and NASA's Planetary Geology and Geophysics Program. P.D.C. acknowledges support by an Australian Postgraduate Award.

ABBREVIATIONS

HST, Hubble Space Telescope; MJQ, Matich-Johnson-Quickenden; NIMS, Near Infrared Mapping Spectrometer; UV, ultraviolet.

REFERENCES

- Ayotte, P., Smith, R.S., Stevenson, K.P., Dohna'lek, Z., Kimmel, G.A., and Kay, B.D. (2001) Effect of porosity on the adsorption, desorption, trapping, and release of volatile gases by amorphous solid water. *J. Geophys. Res.* 106(E12), 33387–33392.
- Bahr, D.A., Famá, M., and Baragiola, R.A. (2001) Radiolysis of water ice in the outer solar system: sputtering and trapping of radiation products. *J. Geophys. Res.* 106, 33285–33290.
- Baragiola, R.A. (2003) Microporous amorphous water ice films and astronomical implications. In *Water in Condensing Geometries*, edited by J.P. Devlin and B. Buch, Elsevier, New York, in press.
- Baragiola, R.A. and Bahr, D.A. (1998) Laboratory studies of the optical properties and stability of oxygen on Ganymede. *J. Geophys. Res.* 103, 25865–25872.
- Baragiola, R.A., Atteberry, C.L., and Bahr, D.A. (1999) Origin of solid oxygen on Ganymede. Reply to comment by R.E. Johnson on "Laboratory studies of the optical properties and stability of oxygen on Ganymede." *J. Geophys. Res.* E104, 14183–14187.
- Baragiola, R.A., Vidal, R.A., Svendsen, W., Schou, J., Shi, M., Bahr, D.A., and Atteberry, C.L. (2003) Sputtering of water ice. *Nucl. Instrum. Methods Phys. Res. B* 209, 294–303.
- Bar-Nun, A., Herman, G., Laufer, D., and Rappaport, M.L. (1985) Trapping and release of gases by water ice and implications for icy bodies. *Icarus* 63, 317–332.
- Baverstock, K.F. and Burns, W.G. (1976) Primary production of oxygen from irradiated water as an explanation for decreased radiobiological oxygen enhancement at high LET. *Nature* 260, 316–318.
- Benit, J. and Brown, W.L. (1990) Electronic sputtering of oxygen and water molecules from thin films of water ice bombarded by MeV Ne^+ ions. *Nucl. Instrum. Methods Phys. Rev. B* 46, 448–451.
- Benit, J., Bibring, J.-P., della-Negra, S., LeBeyec, Y., Mendenhall, M., Rocard, F., and Standing, K. (1987) Erosion of ices by ion irradiation. *Nucl. Instrum. Methods Phys. Rev. B* 19/20, 838–842.
- Brown, W.L., Augustyniak, W.M., Lanzerotti, L.J., Johnson, R.E., and Evatt, R. (1980) Linear and nonlinear processes in the erosion of H_2O ice by fast light ions. *Phys. Rev. Lett.* 43, 1632–1635.
- Brown, W.L., Augustyniak, W. M., Simmons, E., Marcantonio, K.J., Lanzerotti, L.J., Johnson, R.E., Boring, J.W., Reimann, C.T., Foti, G., and Pirronello, V. (1982) Erosion and molecular formation in condensed gas films by electronic energy loss of fast ions. *Nucl. Instrum. Methods B* 1, 307–314.
- Brown, W.L., Augustyniak, W.M., Marcantonio, K.J., Simmons, E.N., Boring, J.W., Johnson, R.E., and Reimann, C.T. (1984) Electronic sputtering of low-temperature molecular solids. *Nucl. Instrum. Methods B* 1, 307.
- Buratti, B. (1995) Photometry and surface structure of the icy Galilean satellites. *J. Geophys. Res.* 100(E9), 19061–19066.
- Buratti, B. and Veverka, J. (1983) Voyager photometry of Europa. *Icarus* 55, 93–110.
- Calvin, W.M. and Spencer, J.R. (1997) Latitudinal distribution of O_2 on Ganymede: observations with the Hubble Space Telescope. *Icarus* 130, 505–516.
- Calvin, W.M., Clark, R.N., Brown, R.H., and Spencer, J.A. (1995) Spectra of the icy Galilean satellites from 0.2 to 5 μm : a compilation, new observations and a recent summary. *J. Geophys. Res.* 100, 19041–19048.
- Calvin, W.M., Johnson, R.E., and Spencer, J.A. (1996) O_2 on Ganymede: spectral characteristics and plasma formation mechanisms. *Geophys. Res. Lett.* 23, 673–676.
- Calvin, W.M., Aninich, V.G., and Brown, R.H. (2004) Oxygen: temperature and phase effects. *Icarus* (in press).

- Carlson, R.W., Anderson, M.S., Johnson, R.E., Smythe, W.D., Hendrix, A.R., Barth, C.A., Soderblom, L.A., Hansen, G.B., McCord, T.B., Dalton, J.B., Clark, R.N., Shirley, J.H., Ocampo, A.C., and Matson, D.L. (1999a) Hydrogen peroxide on the surface of Europa. *Science* 283, 2062–2064.
- Carlson, R.W., Johnson, R.E., and Anderson, M.S. (1999b) Sulfuric acid on Europa and the radiolytic sulfur cycle. *Science* 286, 97–99.
- Carlson, R.W., Anderson, M.S., Johnson, R.E., Schulman, M.B., and Yavrouian, A.H. (2002) Sulfuric acid production on Europa: the radiolysis of sulfur in water ice. *Icarus* 157, 456–463.
- Carlson, R.W., Anderson, M.S., and Johnson, R.E. (2004) Radiolytic carbon compounds on Callisto. *Geophys. Res. Lett.* (in press).
- Carr, M.H., Belton, M.J.S., Chapman, C.R., Davies, M.E., Geissler, P., Greenberg, R., McEwen, A.S., Tufts, B.R., Greeley, R., Sullivan, R., Head, J.W., Pappalardo, R.T., Klaasen, K.P., Johnson, T.V., Kaufan, J., Senske, D., Moore, J., Neukum, G., Schubert, G., Burns, J.A., Thomas, P., and Veverka, J. (1998) Evidence for a sub-surface ocean on Europa. *Nature* 391, 363–365.
- Chyba, C.F. (2000) Energy for microbial life on Europa. *Nature* 403, 381–382.
- Chyba, C.F. and Hand, K.P. (2001) Planetary science—life without photosynthesis. *Science* 292, 2026–2027.
- Cooper, J.F., Johnson, R.E., Mauk, B.H., Garrett, H.B., and Gehrels, N. (2001) Energetic ion and electron irradiation of the icy Galilean satellites. *Icarus* 149, 133–159.
- Cooper, P.D., Johnson, R.E., and Quickenden, T.I. (2003a) A review of the possible optical absorption features of oxygen molecules in the icy surfaces of outer solar system bodies. *Planet Space Sci.* 51, 183–192.
- Cooper, P.D., Johnson, R.E., and Quickenden, T.I. (2003b) Hydrogen peroxide dimers and the production of O₂ in icy satellite surfaces. *Icarus* 166, 444–446.
- Delitsky, M.L. and Lane, A.L. (1998) Ice chemistry on the Galilean satellites. *J. Geophys. Res.* 103, 31391–31403.
- Domingue, D.L. and Hapke, B.W. (1992) Disk-resolved photometric analysis of European terrains. *Icarus* 99, 70–81.
- Domingue, D.L. and Hendrix, A. (2004) Temporal variability in the surface chemistry of the icy Galilean satellites. *Icarus* (in press).
- Domingue, D.L., Hapke, B.W., Lockwood, G.W., and Thompson, D.T. (1991) Europa's phase curve: implications for surface structure. *Icarus* 90, 30–42.
- Engdahl, A. and Nelanders, B. (2002) The dimmer in a too tight matrix cage. *Phys. Chem. Chem. Phys.* 4, 2140–2143.
- Fanale, F.P., Granahan, J.C., McDord, T.B., Hansen, G., Hibbitts, C.A., Carlson, R., Matson, D., Ocampo, A., Kamp, L., Smythe, W., Leader, F., Mehlman, R., Greeley, R., Sullivan, R., Geissler, P., Barth, C., Hendrix, A., Clark, B., Helfenstein, P., Veverka, J., Belton M.J.S., Becker, K., Becker, T., and the Galileo NIMS, SSI, UVS Instrument Teams (1999) Galileo's multiinstrument spectral view of Europa's surface composition. *Icarus* 139, 179–188.
- Geissler, P.E., Greenberg, R., Hoppa, G., McEwen, A., Tufts, R., Phillips, C., Clark, B., Ockert-Bell, M., Helfenstein, P., Burns, J., Veverka, J., Sullivan, R., Greeley, R., Pappalardo, R.T., Head, J.W., Belton, M.S.J., and Denk, T. (1998) Evolution of lineaments on Europa: clues from Galileo multispectral imaging observations. *Icarus* 135, 107–126.
- Gerakines, P.A., Schutte, W.A., and Ehrenfreund, P. (1996) Ultraviolet processing of interstellar ice analogs. 1. Pure ices. *Astron. Astrophys.* 312, 289–305.
- Ghormley, J.A. and Stewart, A.C. (1956) Effects of γ radiation on ice. *J. Am. Chem. Soc.* 78, 2934–2939.
- Gomis, O., Satorre, M.A., Leto, G., and Strazzulla, G. (2004) Hydrogen peroxide formation by ion implantation in water ice and its relevance to the Galilean. *Planet. Space Sci.* (in press).
- Grundy, W.M., Spencer, J.R., and Buie, M.W. (2001) Thermal inertia of Europa's H₂O ice surface component. *Bull. Am. Astron. Soc.* DPS #33, #47.06.
- Gurman, V., Batyuk, V., and Sergeev, G. (1967) Photolysis of frozen dilute solutions of hydrogen peroxide in water. *Kinet. Katal.* 8, 527–531.
- Hall, D.T., Strobel, D.F., Feldman, P.D., McGrath, M.A., and Weaver, H.A. (1995) Detection of an oxygen atmosphere on Jupiter's moon Europa. *Nature* 373, 677–679.
- Hall, D.T., Feldman, P.D., McGrath, M.A., and Strobel, D.F. (1998) The far-ultraviolet oxygen airglow of Europa and Ganymede. *Astrophys. J.* 499, 475–481.
- Hansen, G.B. and McCord, T.B. (1999) Amorphous and crystalline ice on the Galilean satellites: a balance between thermal and radiolytic processes [abstract 1630]. In *Lunar and Planetary Science Conference XXXI* [book on CD-ROM], Lunar and Planetary Institute, Houston.
- Hansen, G.B. and McCord, T.B. (2000) The distribution of amorphous and crystalline ice on Ganymede. *Bull. Am. Astron. Soc.* DPS #32, #39.03H.
- Hart, E.J. and Platzman, R.L. (1961) Radiation chemistry [abstract 1630120]. In *Physical Mechanisms in Radiation Biology I*, edited by M. Erreva and M.A. Forssberg, Academic Press, New York, p. 99.
- Hendrix, A.R., Barth, C.A., and Hord, C.W. (1999a) Ganymede's ozone-like absorber: observations by the Galileo ultraviolet spectrometer. *J. Geophys. Res.* 104(E6), 14169–14178.
- Hendrix, A.R., Barth, C.A., Stewart, A.I.F., Hord, C., and Lane, A.L. (1999b) Hydrogen peroxide on the icy Galilean satellites [abstract 2043]. In *Lunar and Planetary Science Conference XXX* [book on CD-ROM], Lunar and Planetary Institute, Houston.
- Hori, A. and Hondoh, T. (2002) Theoretical study on the diffusion of gases in ice I_h by the molecular orbital method [abstract A-1046]. In *Abstract Conference on the Physics and Chemistry of Ice*, National Research Council of Canada, Montreal.
- Ip, W.-H. (1996) Europa's oxygen exosphere and its magnetosphere interaction. *Icarus* 120, 317–325.
- Johnson, R.E. (1989) Sputtering of a planetary regolith. *Icarus* 78, 206–210.
- Johnson, R.E. (1990) *Energetic Charged-Particle Interactions with Atmospheres and Surface*, Springer-Verlag, Berlin.

- Johnson, R.E. (1998) Sputtering and desorption from icy surfaces. In *Solar System Ices*, edited by B. Schmitt and C. deBergh, Kluwer, Dordrecht, The Netherlands, pp. 303–334.
- Johnson, R.E. (1999) Comment on “Laboratory Studies of the Optical Properties and Stability of Oxygen on Ganymede” by R.A. Baragiola and D.A. Bahr. *J. Geophys. Res.* 104(E6), 14179–14182.
- Johnson, R.E. (2001) Surface chemistry in the Jovian magnetosphere radiation environment. In *Advances Series in Physical Chemistry, Vol. 11: Chemical Dynamics in Extreme Environments*, edited by R. Dessler, World Scientific, Singapore, pp. 390–419.
- Johnson, R.E. and Jesser, W.A. (1997) O₂/O₃ microatmospheres in the surface of Ganymede. *Astrophys. J. Lett.* 480, L79–L82.
- Johnson, R.E. and Quickenden, T.I. (1997) Photolysis and radiolysis of water ice on outer solar system bodies. *J. Geophys. Res.* 102, 10985–10996.
- Johnson, R.E., Lanzerotti, L.J., and Brown, W.L. (1982) Planetary application of ion-induced erosion of condensed-gas frosts. *Nucl. Instrum. Methods* 198, 147–158.
- Johnson, R.E., Nelson, M., McCord, T.B., and Gradie, J. (1988) Analysis of voyage images of Europa: plasma bombardment. *Icarus* 75, 423–436.
- Johnson, R.E., Carlson, R.W., Cooper, J.F., Paranicas, C., Moore, M.H., and Wong, M. (2003) Radiation effects on the surfaces of the Galilean satellites. In *Jupiter: Satellites, Atmosphere, and Magnetosphere*, edited by F. Bagenal, Cambridge University Press, Cambridge, UK, in press.
- Jurac, S., Johnson, R.E., and Richardson, J.D. (2001) Saturn’s E ring and production of the neutral torus. *Icarus* 149, 384–396.
- Kargel, J.S., Kaye, J.Z., Head J.W. III, Marion, G.M., Sassen, R., Crowley, J.K., Ballesteros, O.P., Grant, S.A., and Hogenboom, D.L. (2000) Europa’s crust and ocean: origin, composition, and prospects for life. *Icarus* 148, 226–265.
- Khriachtchev, L., Pettersson, M., Jolkkonen, S., Pehkonen, S., and Rasanen, M. (2000) Photochemistry of hydrogen peroxide in Kr and Xe matrixes. *J. Chem. Phys.* 112, 2187–2194.
- Khusnatdinov, N.N. and Petrenko, V.F. (1992) Photoluminescence of ice I_h in a spectral region 180–300nm. In *Physics and Chemistry of Ice*, edited by N. Maeno and T. Hondoh, Hokkaido University Press, Sapporo, pp. 163–169.
- Kimmel, G.A. and Orlando, T.M. (1995) Low-energy (5–120 eV) electron stimulated dissociation of amorphous D₂O ice: D(²S), O(³P_{2,2,0}), and O(¹D) yields and velocity distributions. *Phys. Rev. Lett.* 75, 2606–2609.
- Kimmel, G.A., Orlando, T.M., Vizina, C., and Sanche, L. (1994) Low energy electron-stimulated production of molecular hydrogen from amorphous water ice. *J. Chem. Phys.* 101, 3282–3286.
- Landau, A., Allis, E.J., and Welsh, H.L. (1962). The absorption spectrum of solid oxygen in the wavelength region from 12,000 Å to 3300 Å. *Spectrochimica Acta* 18, 1–19.
- Langford, V.S., McKinley, A.J. and Quickenden, T.I. (2000) Identification of H₂O-HO in argon matrices. *J. Am. Chem. Soc.* 122, 12859–12863.
- Leblanc, F., Johnson, R.E., and Brown, W.L. (2002) Europa’s sodium atmosphere: an ocean source? *Icarus* 159, 132–144.
- Lefort, M. (1955) Chimie des radiations des solutions aqueuses. In *Actions Chimiques et Biologiques des Radiations, Vol. 1*, edited by M. Haissinsky, Masson, Paris, pp. 203–247.
- Leto, G. and Baratta, G.A. (2003) Lyman alpha photon induced amorphization of Ic water ice at 16 K. Effects and quantitative comparison with ion irradiation. *Astron. Astrophys.* 397, 7–13.
- Livingston, F.E., Smith, J.A., and George, S.M. (2002) General trends for bulk diffusion in ice and surface diffusion on ice. *J. Phys. Chem. A* 106, 6309–6318.
- Madey, T.E., Johnson, R.E., and Orlando, T.M. (2002) Far-out surface science: radiation-induced surface processes in the solar system. *Surf. Sci.* 500, 838–858.
- Matich, A.J., Bakker, M.G., Lennon, D., Quickenden, T.I., and Freeman, C.G. (1993) O₂ luminescence from UV-excited H₂O and D₂O ices. *J. Phys. Chem.* 97, 10539–10553.
- Mauk, B.H., Gary, S.A., Kane, M., Keath, E.P., Krimigis, S.M., and Armstrong, T.P. (1996) Hot plasma parameters of Jupiter’s inner magnetosphere. *Geophys. Res.* 101, 7685–7696.
- McCord, T.B., Hansen, G.B., Matson, D.L., Johnson, T.V., Crowley, J.K., Fanale, F.P., Carlson, R.W., Smythe, W.D., Martin, P.D., Hibbitts, C.A., Granahan, J.C., Ocampo, A., and the NIMS Team (1999) Hydrated salt minerals on Europa’s surface from the Galileo NIMS investigation. *J. Geophys. Res.* 104, 11827–11851.
- McEwen, A.S. (1986) Exogenic and endogenic albedo and color patterns on Europa. *J. Geophys. Res.* 91, 8077–8097.
- McGrath, M.A., Feldman, P.D., Strobel, D.F., Retherford, K., Wolven, B., and Moos, H.W. (2000) HST/STIS Ultraviolet imaging of Europa. *Bull. Am. Astron. Soc. DPS* #32, #34.09.
- Moore, M.H. and Hudson, R.L. (2000) IR detection of H₂O₂ at 80 K in ion-irradiated laboratory ices relevant to Europa. *Icarus* 145, 282–288.
- Noll, K.S., Johnson, R.E., Lane, A.L., Dominigue, D.L., and Weaver, H.A. (1996) Detection of ozone on Ganymede. *Science* 273, 341–343.
- Noll, K.S., Rousch, T.L., Cruikshank, D.P., Johnson, R.E., and Pendleton, Y.J. (1997) Detection of ozone on Saturn’s satellites Rhea and Dione. *Nature* 388, 45–47.
- Orlando, T.M. and Sieger, M.T. (2003) The role of electron-stimulated production of O₂ from water ice in the radiation processing of outer solar system surfaces. *Surf. Sci.* 528, 1–7.
- Orlando, T.M., Sieger, M.T., and Simpson, W.C. (1998) Laboratory studies of the production of O₂ on icy satellites by electronic excitation [abstract 1394]. In *Lunar and Planetary Science Conference XXX* [book on CD-ROM], Lunar and Planetary Institute, Houston.
- Paranicas, C., Carlson, R.W., and Johnson, R.E. (2001) Electron bombardment of Europa. *Geophys. Res. Lett.* 28, 673–676.

- Paranicas, C., Ratliff, J.M., Mauk, B.H., Cohen, C., and Johnson, R.E. (2002) The ion environment near Europa and its role in surface energetics. *Geophys. Res. Lett.* 29, 14127.
- Prockter, L.M. and Pappalardo, R.T. (2000) Folds on Europa: implications for crustal cycling and accommodation of extension. *Science* 289, 941–943.
- Reimann, C.T., Boring, J.W., Johnson, R.E., Garrett, J.W., and Farmer, K.R. (1984) Ion-induced molecular ejection from D₂O ice. *Surf. Sci.* 147, 227–240.
- Rowland, B., Fisher, M., and Devlin, J.P. (1991) Probing icy surfaces with the dangling-OH-mode absorption: large ice clusters and microporous amorphous ice. *J. Chem. Phys.* 95, 1378–1384.
- Ruiz, J. and Tejero, R. (2000) Heat flows through the ice lithosphere of Europa. *J. Geophys. Res.* 105(E12), 29283.
- Rye, R.R., Madey, T.E., Houston, J.E., and Holloway, P.H. (1978) Chemical-state effects in Auger electron spectroscopy. *J. Chem. Phys.* 69, 1504–1512.
- Selby, B. (2003) A kinetic study of UV-excited ice luminescence [Ph.D. Thesis], University of Western Australia, Perth.
- Shematovich, V.I. and Johnson, R.E. (2001) Near-surface oxygen atmosphere at Europa. *Adv. Space Res.* 27, 1881–1888.
- Sieger, M.T., Simpson, W.C., and Orlando, T.M. (1998) Production of O₂ on icy satellites by electronic excitation of low-temperature water ice. *Nature* 394, 554.
- Smith, R.S. and Kay, B.D. (1997) Adsorption, desorption and crystallization kinetics in nanoscale water films. *Recent Res. Dev. Phys. Chem.* 1, 209–219.
- Spencer, J.R. and Calvin, W.M. (2002) Condensed O₂ on Europa and Callisto. *Astron. J.* 124, 3400–3403.
- Spencer, J.R. and Klesman, A. (2001) New observations of molecular oxygen on Europa and Ganymede. *Bull. Am. Astron. Soc.* DPS #33, #47.04.
- Spencer, J.R., Calvin, W., and Person, J. (1995) CCD spectra of the Galilean satellites: molecular oxygen on Ganymede. *J. Geophys. Res.* 100, 19049–19056.
- Strazzulla, G. (1998) Chemistry of ice induced by energetic charged particles. In *Solar System Ices*, edited by B. Schmitt and C. deBergh, Kluwer, Dordrecht, The Netherlands, pp. 281–302.
- Taub, I.A. and Eiben, K. (1968) Transient solvated electron, hydroxyl, and hydroperoxy radicals in pulse-irradiated crystalline ice. *J. Chem. Phys.* 49, 2499–2513.
- Vaghjiani, G.L., Turnipseed, A.A., Warren, R.F., and Ravishankara, A.R. (1992) Photodissociation of H₂O₂ at 193 and 222 nm: products and quantum yields. *J. Chem. Phys.* 96, 5878–5886.
- Watanabe, N. and Kouchi, A. (2002) Measurements of conversion rates of CO to CO₂ in ultraviolet-induced reaction of D₂O(H₂O)/CO amorphous ice. *Astrophys. J.* 567, 651–655.
- Watanabe, N., Horii, T., and Kouchi, A. (2000) Measurements of D₂ yields from amorphous D₂O ice by ultraviolet irradiation at 12K. *Astrophys. J.* 541, 772–778.
- Westley, M.S., Bargioli, R.A., Johnson, R.E., and Baratta, G.A. (1995) Ultraviolet photodesorption from water ice. *Planet. Space Sci.* 43, 1311–1315.
- Williams, T.L., Adams, N.G., Babcock, L.M., Herd, C.R. and Geoghegan, M. (1996) Production and loss of the water-related species H₃O⁺, H₂O and OH in dense interstellar clouds. *Monthly Notices R. Soc.* 282, 413–420.

Address reprint requests to:

Dr. R.E. Johnson
Engineering Physics
Thornton Hall B103
University of Virginia
Charlottesville, VA 22904

E-mail: rej@virginia.edu

This article has been cited by:

1. M. H. Burger, E. C. Sittler, R. E. Johnson, H. T. Smith, O. J. Tucker, V. I. Shematovich. 2007. Understanding the escape of water from Enceladus. *Journal of Geophysical Research* **112**:a6, A06219. [[CrossRef](#)]
2. Reggie L. Hudson , Marla H. Moore . 2006. Infrared Spectra and Radiation Stability of H₂O₂ Ices Relevant to Europa. *Astrobiology* **6**:3, 483-489. [[Abstract](#)] [[PDF](#)] [[PDF Plus](#)]
3. Kevin P. Hand , Christopher F. Chyba , Robert W. Carlson , John F. Cooper . 2006. Clathrate Hydrates of Oxidants in the Ice Shell of Europa. *Astrobiology* **6**:3, 463-482. [[Abstract](#)] [[PDF](#)] [[PDF Plus](#)]
4. Nikolay G. Petrik, Alexander G. Kavetsky, Greg A. Kimmel. 2006. Electron-stimulated production of molecular oxygen in amorphous solid water on Pt(111): Precursor transport through the hydrogen bonding network. *The Journal of Chemical Physics* **125**:12, 124702. [[CrossRef](#)]
5. Prof. G. Strazzulla , G. Leto , F. Spinella , O. Gomis . 2005. Production of Oxidants by Ion Irradiation of Water/Carbon Dioxide Frozen Mixtures. *Astrobiology* **5**:5, 612-621. [[Abstract](#)] [[PDF](#)] [[PDF Plus](#)]
6. H. Luna, C. McGrath, M. B. Shah, R. E. Johnson, M. Liu, C. J. Latimer, E. C. Montenegro. 2005. Dissociative Charge Exchange and Ionization of O₂ by Fast H⁺ and O⁺ Ions: Energetic Ion Interactions in Europa's Oxygen Atmosphere and Neutral Torus. *The Astrophysical Journal* **628**:2, 1086. [[CrossRef](#)]
7. R. E. Johnson, M. Liu, E. C. Sittler. 2005. Plasma-induced clearing and redistribution of material embedded in planetary magnetospheres. *Geophysical Research Letters* **32**:24, L24201. [[CrossRef](#)]
8. R. E. Johnson, P. D. Cooper, T. I. Quickenden, G. A. Grieves, T. M. Orlando. 2005. Production of oxygen by electronically induced dissociations in ice. *The Journal of Chemical Physics* **123**:18, 184715. [[CrossRef](#)]